



# A Mini-Neptune from TESS and CHEOPS Around the 120 Myr Old AB Dor Member HIP 94235

George Zhou<sup>1</sup> , Christopher P. Wirth<sup>2,3</sup> , Chelsea X. Huang<sup>1</sup> , Alexander Venner<sup>4</sup> , Kyle Franson<sup>5</sup>, Samuel N. Quinn<sup>3</sup> , L. G. Bouma<sup>6,28</sup> , Adam L. Kraus<sup>7</sup> , Andrew W. Mann<sup>8</sup> , Elisabeth. R. Newton<sup>9</sup> , Diana Dragomir<sup>10</sup> , Alexis Heitzmann<sup>1</sup> , Natalia Lowson<sup>1</sup> , Stephanie T. Douglas<sup>11</sup> , Matthew Battley<sup>12,13</sup> , Edward Gillen<sup>14,15,29</sup> , Amaury Triaud<sup>16</sup> , David W. Latham<sup>3</sup> , Steve B. Howell<sup>17</sup> , J. D. Hartman<sup>18</sup> , Benjamin M. Tofflemire<sup>7</sup> , Robert A. Wittenmyer<sup>1</sup> , Brendan P. Bowler<sup>5</sup> , Jonathan Horner<sup>1</sup> , Stephen R. Kane<sup>19</sup> , John Kielkopf<sup>20</sup> , Peter Plavchan<sup>21</sup> , Duncan J. Wright<sup>1</sup> , Brett C. Addison<sup>1</sup> , Matthew W. Mangel<sup>1</sup> , Jack Okumura<sup>1</sup>, George Ricker<sup>22</sup> , Roland Vanderspek<sup>22</sup> , Sara Seager<sup>22,23,24</sup> , Jon M. Jenkins<sup>17</sup> , Joshua N. Winn<sup>25</sup> , Tansu Daylan<sup>22,26</sup> , Michael Fausnaugh<sup>22</sup> , and Michelle Kunimoto<sup>27</sup>

<sup>1</sup> University of Southern Queensland, Centre for Astrophysics, West Street, Toowoomba, QLD 4350 Australia; [george.zhou@usq.edu.au](mailto:george.zhou@usq.edu.au)

<sup>2</sup> Harvard University, Cambridge, MA 02138, USA

<sup>3</sup> Center for Astrophysics | Harvard & Smithsonian, 60 Garden Street, Cambridge, MA 02138, USA

<sup>4</sup> University of Southern Queensland, Centre for Astrophysics, West Street, Toowoomba, QLD 4350, Australia

<sup>5</sup> Department of Astronomy, The University of Texas at Austin, TX 78712, USA

<sup>6</sup> Cahill Center for Astrophysics, California Institute of Technology, Pasadena, CA 91125, USA

<sup>7</sup> Department of Astronomy, The University of Texas at Austin, Austin, TX 78712, USA

<sup>8</sup> Department of Physics and Astronomy, The University of North Carolina at Chapel Hill, Chapel Hill, NC 27599, USA

<sup>9</sup> Department of Physics and Astronomy, Dartmouth College, Hanover, NH 03755, USA

<sup>10</sup> Department of Physics and Astronomy, University of New Mexico, 210 Yale Boulevard NE, Albuquerque, NM 87106, USA

<sup>11</sup> Department of Physics, Lafayette College, 730 High Street, Easton, PA 18042, USA

<sup>12</sup> Department of Physics, University of Warwick, Gibbet Hill Road, Coventry CV4 7AL, UK

<sup>13</sup> Centre for Exoplanets and Habitability, University of Warwick, Gibbet Hill Road, Coventry CV4 7AL, UK

<sup>14</sup> Astronomy Unit, Queen Mary University of London, Mile End Road, London E1 4NS, UK

<sup>15</sup> Astrophysics Group, Cavendish Laboratory, J.J. Thomson Avenue, Cambridge CB3 0HE, UK

<sup>16</sup> School of Physics & Astronomy, University of Birmingham, Edgbaston, Birmingham, B15 2TT, UK

<sup>17</sup> NASA Ames Research Center, Moffett Field, CA 94035, USA

<sup>18</sup> Department of Astrophysical Sciences, Princeton University, 4 Ivy Lane, Princeton, NJ 08540, USA

<sup>19</sup> Department of Earth and Planetary Sciences, University of California, Riverside, CA 92521, USA

<sup>20</sup> Department of Physics and Astronomy, University of Louisville, Louisville, KY 40292, USA

<sup>21</sup> George Mason University, 4400 University Drive MS 3F3, Fairfax, VA 22030, USA

<sup>22</sup> Department of Physics and Kavli Institute for Astrophysics and Space Research, Massachusetts Institute of Technology, Cambridge, MA 02139, USA

<sup>23</sup> Department of Earth, Atmospheric and Planetary Sciences, Massachusetts Institute of Technology, Cambridge, MA 02139, USA

<sup>24</sup> Department of Aeronautics and Astronautics, MIT, 77 Massachusetts Avenue, Cambridge, MA 02139, USA

<sup>25</sup> Department of Astrophysical Sciences, Princeton University, Princeton, NJ 08544, USA

<sup>26</sup> Department of Astrophysical Sciences, Princeton University, Peyton Hall, Princeton, NJ 08544, USA

<sup>27</sup> Kavli Institute for Astrophysics and Space Research, Massachusetts Institute of Technology, Cambridge, MA 02139, USA

Received 2022 March 28; revised 2022 April 14; accepted 2022 April 22; published 2022 May 24

## Abstract

The Transiting Exoplanet Survey Satellite (TESS) mission has enabled discoveries of the brightest transiting planet systems around young stars. These systems are the benchmarks for testing theories of planetary evolution. We report the discovery of a mini-Neptune transiting a bright star in the AB Doradus moving group. HIP 94235 (TOI-4399, TIC 464646604) is a  $V_{\text{mag}} = 8.31$  G-dwarf hosting a  $3.00_{-0.28}^{+0.32} R_{\oplus}$  mini-Neptune in a 7.7 day period orbit. HIP 94235 is part of the AB Doradus moving group, one of the youngest and closest associations. Due to its youth, the host star exhibits significant photometric spot modulation, lithium absorption, and X-ray emission. Three 0.06% transits were observed during Sector 27 of the TESS Extended Mission, though these transit signals are dwarfed by the 2% peak-to-peak photometric variability exhibited by the host star. Follow-up observations with the Characterising Exoplanet Satellite confirmed the transit signal and prevented the erosion of the transit ephemeris. HIP 94235 is part of a 50 au G-M binary system. We make use of diffraction limited observations spanning 11 yr, and astrometric accelerations from Hipparcos and Gaia, to constrain the orbit of HIP 94235 B. HIP 94235 is one of the tightest stellar binaries to host an inner planet. As part of a growing sample of bright, young planet systems, HIP 94235 b is ideal for follow-up transit observations, such as those that investigate the evaporative processes driven by high-energy radiation that may sculpt the valleys and deserts in the Neptune population.

<sup>28</sup> 51 Pegasi b Fellow.

<sup>29</sup> Winton Fellow.



*Unified Astronomy Thesaurus concepts:* [Exoplanet astronomy \(486\)](#); [Exoplanet evolution \(491\)](#); [Exoplanet detection methods \(489\)](#)

## 1. Introduction

Young planets offer a time-lapse view of the construction of the exoplanet demographics. Planetary systems are thought to undergo rapid evolution within the first hundreds of millions of years after their formation. Follow-up characterization of small young planets helps to test our models for the contraction and mass-loss processes that they undergo during this time frame.

Thousands of close-in Neptunes and super-Earths were discovered by the primary Kepler mission (e.g., Petigura et al. 2013; Burke et al. 2015; Zhu et al. 2018). The mechanisms that sculpted the period–radius distribution of these planets can shed light on the early formation and evolution of planetary systems. The evaporation of primordial hydrogen and helium envelopes, driven by UV and X-ray radiation from young stars, can reproduce the sub-Neptune desert and radius valley (e.g., Lopez et al. 2012; Owen & Wu 2013, 2017). These processes act on rapid timescales because the high-energy fluxes from young stars rapidly decline over time. Mass loss can also be driven by heat leaking out from a planet’s deep interior, a process that can last hundreds of millions of years as the planets cool down after accretion (e.g., Lopez & Fortney 2013; Ginzburg et al. 2018; Gupta & Schlichting 2021). Giant impacts within compact super-Earth and Neptune systems may erode the envelopes of some planets, occurring after disk dissipation and before the systems dynamically cool within the first hundred million years (e.g., Marcus et al. 2009; Inamdar & Schlichting 2015). As their primordial gaseous envelopes are stripped away, it is possible that some planets lying in less energetic environments may be replenished by secondary atmospheres (e.g., Kite & Barnett 2020). Other mechanisms, such as in situ formation in gas-poor disks, may naturally carve out the current period–radius distribution of small planets (Lee & Connors 2021; Lee et al. 2022), and the radii of small planets may evolve much slower than predicted from runaway mass-loss models (David et al. 2021).

Young planets can help establish the timescales for the evolution of the period–radius distribution of the super-Earth and Neptune populations. For some planets, mass loss through photoevaporation occurs throughout their lifetime without significantly changing their radii. Extended atmospheres have been observed for Neptune-sized planets about older field stars in X-rays (Ehrenreich et al. 2012), Ly $\alpha$  (Kulow et al. 2014; Ehrenreich et al. 2015; Lavie et al. 2017; Bourrier et al. 2018), and He I (Spake et al. 2018; Allart et al. 2019; Kirk et al. 2020). However, for planets between 2 and 4  $R_{\oplus}$ , runaway evaporation may occur. This process strips away the outer primordial envelope of these Neptunes and super-Earths, leaving behind rocky cores. Real-time measurements of photoevaporation for younger systems can help establish the timescale for this process and its influence on the radius evolution of planets. Zhang et al. (2022b) detected the Ly $\alpha$  transit of the outer planet HD 63433 c in a 400 Myr old planetary system. They also reported the lack of a detectable escaping hydrogen atmosphere for the inner planet, suggesting that it may have already undergone runaway evaporation and lost its primordial atmosphere. Rockcliffe et al. (2021) reported a nondetection of escaping hydrogen for the 650 Myr old K2-25b, with one possibility for the nondetection being factors related to the

star’s youth. Zhang et al. (2022a) reported escaping He I for the 500 Myr old mini-Neptune HD 73583 b, showing an excess 0.68% absorption for the He I 10830 Å line. Tentative detections of atmospheric escape have been reported for planets in the V1298 Tau system in Ca II, H- $\alpha$  (Feinstein et al. 2021), and He I (Gaidos et al. 2022).

The K2 mission (Howell et al. 2014) yielded some of the first young transiting planets (e.g., Mann et al. 2016a, 2016b; David et al. 2016; Rizzuto et al. 2018; Vanderburg et al. 2018; David et al. 2019a, 2019b; Livingston et al. 2019; Barragán et al. 2019), and provided insight into the radius distribution of these planets compared to those about older stars (e.g., Rizzuto et al. 2017; David et al. 2021). The Transiting Exoplanet Survey Satellite (TESS) mission (Ricker et al. 2015) is finding young planets that are more suitable for in-depth characterization: DS Tuc A (Newton et al. 2019), HD 63433 (Mann et al. 2020), and AU Mic (Plavchan et al. 2020) are among the brightest planet-hosting stars known. These are the best targets for in-depth follow-up studies with the suite of new astronomical observatories coming online this decade.

In this paper, we present the discovery of a mini-Neptune-sized planet transiting the  $V = 8.3$  star HIP 94235, a member of the  $\sim 120$  Myr old AB Doradus moving group, one of the youngest and closest stellar associations. HIP 94235 was identified as a planet host through a search for planets around active stars (Zhou et al. 2021). The star’s youth is confirmed from its spectroscopic and photometric characteristics, such as its rapid rotation and significant photometric modulation, strength of lithium absorption, and X-ray emission. The kinematics and independent age estimation of HIP 94235 agree with that of members of the AB Doradus moving group. The shallow 600 ppm transits of HIP 94235 b were identified in the single sector of observations obtained by TESS during the first sector of its ongoing Extended Mission. Subsequent observations via the CHAracterising ExOPlanet Satellite (CHEOPS) space telescope made it possible to confirm the existence of the transits and improved our ability to predict future transit times for follow-up studies.

## 2. Observations

### 2.1. Candidate Identification with TESS

TESS (Ricker et al. 2015) performed photometric measurements of HIP 94235 in its Sector 27 Camera 2 observations between 2020 July 04 and 30. HIP 94235 was observed at two-minute cadence via target pixel stamp observations, and was also included as a target of multiple TESS Guest Investigator Programs (G03251, D. Huber; G03272, J. Burt). We make use of Simple Aperture Photometry light curves (Twicken et al. 2010; Morris et al. 2020) from the Science Processing Observation Center (SPOC; Jenkins et al. 2016), extracted from the two-minute target pixel files for subsequent analyses. The field around HIP 94235 is shown in Figure 1 as seen from ground-based surveys, TESS, and subsequent follow-up observations.

HIP 94235 was identified as a planet candidate by a dedicated search for planets around young stars (Zhou et al. 2021). We first identified HIP 94235 as a possible young star via its rotationally modulated light curve. Three transits were

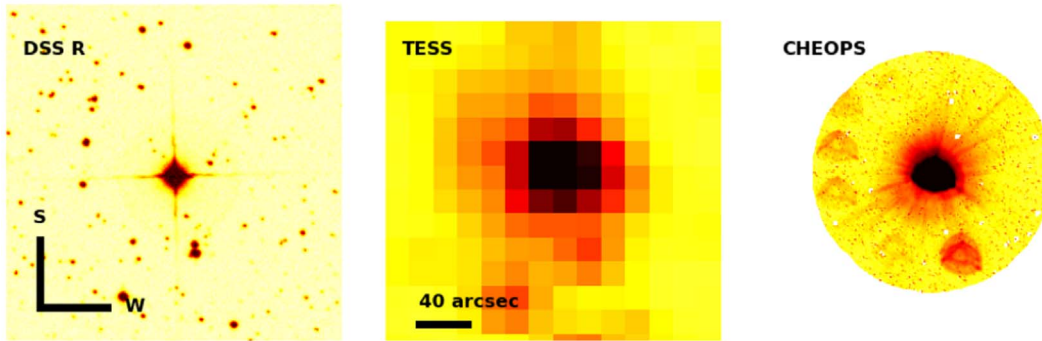


**Figure 1.** Field around HIP 94235 from the Deep Sky Survey *R* band (left), TESS (middle), and CHEOPS (right). The images have approximately the same field sizes ( $5'$ ) and orientations.

identified using a Box-fitting Least Squares search (Kovács et al. 2002) on the light curve after detrending using a high-order spline-fitting procedure (Vanderburg & Johnson 2014). HIP 94235 was also identified as a threshold crossing event in both the SPOC pipeline (Jenkins et al. 2016) and the MIT QuickLook Pipeline (Huang et al. 2020a). The SPOC threshold crossing event diagnostic tests indicate the transit is on target to within  $5''.3 \pm 2''.5$ . However, it did not survive the TESS object of interest (TOI) vetting process initially because of the large amplitude of the residuals in the detrended light curves, which is due to the intrinsic variability of the star. The candidate was promoted to become a TOI after the confirmation of the photometric transit signals using the CHEOPS observations (Section 2.2).

To account for the instrumental noise due to spacecraft motion and stellar variability in the light curves, we perform a simultaneous detrending using the spacecraft quaternions and basis splines following a similar process to that described in Vanderburg et al. (2019). We iteratively fit for linear coefficients of the mean, standard deviation, and skew terms of the three quaternions, together with a spline matrix created by the LIGHTKURVE package (Lightkurve Collaboration et al. 2018). The detrended light curve is adopted for our subsequent analyses in Section 4.

The corrected TESS light curve from Sector 27 is shown in Figure 2. Figure 3 shows close-ups of individual transits of HIP 94235 b in the raw and detrended TESS light curves. Figure 4 shows the phase-folded TESS transit light curve and its best-fit model from our global modeling (Section 4).

## 2.2. Follow-up Photometry with CHEOPS

To confirm the existence and constrain the transit ephemeris of HIP 94235 b, we obtained space-based photometric observations using ESA’s CHEOPS (Benz et al. 2021), through the CHEOPS Guest Observers Programme (AO2-005). CHEOPS is a 0.32 m Ritchey–Chrétien telescope in a nadir-locked 700 km low-Earth orbit, along the Earth’s day/night terminator, with a period of 98.725 minutes. The telescope has a field of view of  $17' \times 17'$  and is instrumentally defocused with a point-spread function of  $16''$  at a plate scale of  $1'' \text{ pixel}^{-1}$ .

A transit of HIP 94235 b was observed by CHEOPS between 2021 August 19 23:59 and 2021 August 20 07:33 UTC (visit ID 1568350). The visit consists of five orbits, with an exposure time of 17 s coadded on board to a cadence of 34 s. The visit had an observing efficiency of 61% (fraction of time on target), with interruptions primarily due to Earth stray light. A total of

498 exposures were obtained, of which, nine exposures were affected by stray light and Earth occultation, eight by South Atlantic Anomaly crossings. An example frame from CHEOPS is shown in Figure 1. The observations were reduced by the CHEOPS Data Reduction Pipeline v13.1.0 (Hoyer et al. 2020), accounting for bias, dark current, flat-fielding, bad pixel correction, smear contamination, and linearization. We adopt the optimal aperture light curve, with a circular aperture of 31 pixels, for our analysis. Aperture contamination by background stars is estimated to be at the  $6 \times 10^{-4}$  level and is accounted for via the simulations from the data reduction pipeline.

The CHEOPS light curve exhibits a smooth hour-long trend that can be attributed to the spot modulated rotational variations of HIP 94235. Shorter timescale instrumental variations associated with the spacecraft roll angle are seen on the orbital timescales (Maxted et al. 2021). We model the spot modulation over the five orbits of observations with a fourth-order polynomial after removal of the transit model. We also fit for a fifth-order correlation between the spacecraft roll angle and the resulting light-curve residuals. This modeling is performed simultaneous to the global fit of the TESS light curve and associated parameters, such that the uncertainties from this detrending process are fully accounted for in our results (Section 4). The raw and corrected CHEOPS light curves are shown in Figure 5, and the binned and corrected phase-folded data are compared with those from TESS in Figure 4.

The CHEOPS observation was most crucial in refining the ephemeris of HIP 94235 b. With a transit depth of 600 ppm, detecting the photometric transit event with ground-based facilities is difficult. With only three transits available during the single sector of TESS observations over the entire primary and first extended mission, the TESS ephemeris would have quickly become stale. The ephemeris uncertainty using TESS observations alone would have been 5.2 hr after five years, making any transit follow-up studies more difficult to schedule. The single CHEOPS transit reduced the five-year transit timing uncertainty to 8 minutes. Figure 6 illustrates the reduction in transit ephemeris uncertainty enabled by the CHEOPS observation.

## 2.3. Clearing of Nearby Eclipsing Binaries from Las Cumbres Observatory

The large TESS and CHEOPS point-spread functions allow for multiple stars within a photometric aperture to be the source of a photometric transit detection. We obtained a transit observation of HIP 94235 b with the Las Cumbres Observatory Global Network (LCOGT; Brown et al. 2013) 1 m telescope at

Las Campanas Observatory on 2021 May 26 UTC. The observations were performed in the  $g'$  band and were defocused to a FWHM of  $7''$  due to the brightness of the target star. The observations showed that no nearby stars visually separable with HIP 94235 within  $1'$  exhibited eclipsing or transiting events during the predicted transit of HIP 94235 b. Though the transit of HIP 94235 b was not detected due to its shallow depth, this LCOGT observation cleared nearby stars of being stellar eclipsing binaries.

#### 2.4. Reconnaissance Spectroscopy

To characterize the target star and confirm its youth spectroscopically, we obtained three observations of HIP 94235 with the High-Resolution Spectrograph (HRS; Crause et al. 2014) on the Southern African Large Telescope (SALT; Buckley et al. 2006) in October 2020. HRS is a fiber-fed echelle spectrograph with a resolving power of  $R \sim 65,000$  over the wavelength range of 3700–8900 Å. Spectral extraction was performed via the MIDAS pipeline (Kniazev et al. 2016, 2017).<sup>30</sup> These observations confirmed the presence of the lithium 6708 Å doublet and strong chromospheric emission in the Calcium H & K line cores. The lack of significant radial velocity variations or secondary sets of spectral lines indicated the transiting candidate was not an obvious blended eclipsing stellar binary system.

We obtained 16 observations of HIP 94235 using the CHIRON fiber-fed cross-dispersed echelle spectrometer at the SMARTS 1.5 m telescope located at the Cerro Tololo Inter-American Observatory, Chile (Tokovinin et al. 2013). CHIRON has a spectral resolving power of  $R = 80,000$  over the wavelength range of 4100–8700 Å. Spectra from CHIRON were reduced as per Paredes et al. (2021). The radial velocities were measured following the procedure from Zhou et al. (2021) via a least-squares deconvolution of each observation against a synthetic nonrotating template generated from the ATLAS9 model atmospheres (Castelli & Kurucz 2004). The radial velocity measurements are presented in Table 1 and Figure 7.

In addition, we follow Zhou et al. (2021) and measure the spectroscopic atmospheric parameters of HIP 94235 from the CHIRON spectra. We match the spectrum of HIP 94235 against an interpolated library of  $\sim 10,000$  observed spectra pre-classified by the spectroscopic classification pipeline (Buchhave et al. 2012), finding that HIP 94235 has an effective temperature of  $5991 \pm 50$  K, surface gravity of  $4.46 \pm 0.02$  dex, and metallicity of  $[M/H] = -0.05 \pm 0.10$  dex. We adopt the spectroscopic effective temperature as a prior in the global modeling described in Section 4.

We also used the MINERVA-Australis telescope array for further reconnaissance of HIP 94235. MINERVA-Australis is an array of four identical 0.7 m CDK700 telescopes located at Mount Kent Observatory, Australia (Addison et al. 2019). The telescopes feed into a single KiwiSpec echelle spectrograph with a spectral resolving power of  $R \approx 80,000$  over the wavelength region of 4800–6200 Å. The instrument is environmentally controlled inside a vacuum chamber, and simultaneous wavelength calibration is provided by two calibration fibers that bracket the science fibers on the detector, each fed from a quartz lamp via an iodine cell. The radial velocities are measured from the extracted spectra as per our CHIRON analyses described above, via a least-squares

**Table 1**  
Radial Velocity Measurements of HIP 94235

BJD	RV (km s <sup>-1</sup> )	RV Error (km s <sup>-1</sup> )	Instrument
2459305.91348	8.131	0.100	CHIRON
2459309.87630	8.211	0.134	CHIRON
2459311.89601	8.220	0.073	CHIRON
2459320.89052	8.152	0.082	CHIRON
2459327.86151	8.246	0.079	CHIRON
2459335.86210	8.340	0.120	CHIRON
2459337.89892	8.123	0.099	CHIRON
2459339.86391	8.144	0.087	CHIRON
2459459.55982	8.069	0.087	CHIRON
2459461.57939	8.255	0.083	CHIRON
2459463.56573	8.285	0.072	CHIRON
2459464.59690	8.273	0.068	CHIRON
2459465.56939	8.271	0.282	CHIRON
2459467.53083	8.394	0.092	CHIRON
2459478.48380	8.459	0.098	CHIRON
2459479.48429	8.123	0.119	CHIRON
2459480.51450	8.355	0.093	CHIRON
2459481.51666	8.466	0.096	CHIRON
2459482.55682	8.350	0.068	CHIRON
2459485.52901	8.485	0.062	CHIRON
2459506.52501	8.237	0.071	CHIRON
2459508.52808	8.107	0.102	CHIRON
2459319.14408	8.841	0.104	MINERVA-Australis Tel 3
2459324.21159	8.964	0.175	MINERVA-Australis Tel 3
2459332.10157	8.914	0.178	MINERVA-Australis Tel 3
2459348.10572	9.096	0.165	MINERVA-Australis Tel 3
2459452.00282	9.152	0.143	MINERVA-Australis Tel 3
2459453.04237	8.976	0.150	MINERVA-Australis Tel 3
2459453.99779	9.120	0.140	MINERVA-Australis Tel 3
2459456.02452	9.171	0.139	MINERVA-Australis Tel 3
2459476.98480	8.961	0.109	MINERVA-Australis Tel 3
2459319.14408	9.208	0.161	MINERVA-Australis Tel 4
2459324.21159	8.766	0.101	MINERVA-Australis Tel 4
2459348.10572	8.995	0.167	MINERVA-Australis Tel 4
2459452.00282	9.177	0.194	MINERVA-Australis Tel 4
2459453.04237	9.017	0.146	MINERVA-Australis Tel 4
2459453.99779	9.265	0.148	MINERVA-Australis Tel 4
2459476.98480	9.121	0.179	MINERVA-Australis Tel 4
2459319.14408	8.955	0.176	MINERVA-Australis Tel 5
2459324.21159	9.085	0.137	MINERVA-Australis Tel 5
2459332.10157	8.741	0.123	MINERVA-Australis Tel 5
2459348.10572	9.077	0.181	MINERVA-Australis Tel 5

deconvolution between the observations and the synthetic nonrotating template. The radial velocities are provided in Table 1.

### 3. Age and Membership

HIP 94235 shares space velocities with the AB Doradus moving group (Section 3.1.1). The age of the group has been estimated to be between 50 and 150 Myr. The group has also been linked to be coevolving with the Pleiades. We adopt an AB Doradus age of 120 Myr for the remainder of this discussion. In addition, a neighborhood search for tangentially comoving stars with HIP 94235 reveals a tentative population of stars, with an age of  $\sim 120$  Myr, determined by their rotation periods. The following sections examine the kinematic properties of HIP 94235 and the association, as well as the photometric and spectroscopic characteristics of HIP 94235 that identify its youth independent of the kinematics.

<sup>30</sup> [http://www.sao.ac.za/~akniazev/pub/HRS\\_MIDAS/HRS\\_pipeline.pdf](http://www.sao.ac.za/~akniazev/pub/HRS_MIDAS/HRS_pipeline.pdf)

**Table 2**  
Candidate Comoving and Coevolving Stars with HIP 94235

TIC	R.A. (deg)	Decl. (deg)	U (km s <sup>-1</sup> )	V (km s <sup>-1</sup> )	W (km s <sup>-1</sup> )	B (mag)	V (mag)	T (mag)	K (mag)	$P_{\text{rot}}$ (d)	Li EW (Å)
71314712	330.63261	-47.67748	-4.0	-26.0	-4.0	9.3	8.8	8.2	7.4	2.4	
91231096	310.66707	-46.67197	-1.9	-26.3	-1.9	11.0	10.0	9.1	7.6	4.6	
93839949	176.15935	-49.41756	-7.3	-24.7	-7.3	9.9	8.9	8.0	6.5	1.9	
101403239	300.79541	-52.96796	-1.7	-26.0	-1.7	12.8	11.9	10.9	9.4	12.7	
108272865	285.27521	-28.71442	-5.2	-27.4	-5.2	9.0	8.5	8.0	7.2	2.4	
142144969	99.73088	-74.42526	-5.2	-26.1	-5.2	10.5	9.7	9.0	7.9	7.0	
197597944	327.20235	-39.48626	-8.5	-28.1	-8.5	10.3	9.7	9.0	8.0	4.1	
206603521	21.80129	-57.29366	-7.9	-26.8	-7.9	14.5	13.0	11.1	8.8	3.8	
234299476	358.66836	-60.85971	-8.3	-27.2	-8.3	11.1	10.0	9.0	7.5	9.0	
270200832	331.81221	-74.08641	-3.0	-26.4	-3.0	9.5	9.0	8.5	7.8	2.0	
270259954	359.04562	-39.05314	-7.5	-27.7	-7.5	9.2	8.2	7.3	5.9	7.8	
270377865	345.08089	-26.15444	-3.1	-26.3	-3.1	8.1	7.5	6.9	5.9	3.6	
278271178	112.29658	-82.20387	-4.4	-24.9	-4.4	14.3	13.1	11.1	8.9	10.9	
280683734	342.73660	-79.16594	-7.5	-27.0	-7.5	9.6	9.0	8.4	7.6	2.6	0.136
290081380	319.52174	-29.52160	-7.0	-29.4	-7.0	15.1	13.9	11.5	9.3	10.3	
341498715	318.52194	-63.70066	-6.9	-27.1	-6.9	10.9	10.1	9.4	8.2	5.9	
357709300	189.06702	-79.52628	-7.3	-26.8	-7.3	12.2	11.0	10.2	8.7	7.0	
369897885	171.32165	-84.95449	-8.4	-25.4	-9.6	8.1	7.6	7.2	6.5	1.5	0.030
389660501	321.33728	-43.51207	-3.5	-25.8	-3.5	13.4	12.1	11.0	9.1	7.1	
405077613	112.74683	-84.32411	-8.6	-27.2	-8.6	10.8	10.0	9.2	7.9	4.9	0.200
409141582	312.08079	-28.02455	-5.7	-27.3	-5.7	13.7	13.6	11.4	9.1	2.7	
409141582	312.08194	-28.02453	-9.2	-25.0	-9.2	13.7	13.6	11.4	9.1	2.7	
439417806	301.15247	-35.21447	-3.7	-26.2	-3.7	9.4	8.9	12.2	7.7	1.4	
464646604	287.74114	-60.27264	-5.7	-27.0	-5.7	8.9	8.3	7.8	6.9	2.2	0.141
466277708	305.70238	-65.25823	-6.9	-27.0	-6.9	10.3	9.6	9.0	8.1	3.8	

As accretion dwindles, young stars spin up as they conserve their angular momentum while they contract in radius. The spin up leads to increased magnetic activity, large photospheric spots, and increased chromospheric activity. Both rotation and activity then decay with time as angular momentum is lost through the stellar wind over the main-sequence lifetime of the star. The TESS light curve of HIP 94235 exhibits significant rotational spot modulation, which first drew our attention to its potential youth. The presence of X-ray emission and lithium absorption for the Sun-like host star confirm its youth. A flare event was also observed during the second orbit of the TESS sector, consistent with the behavior expected for a young star.

### 3.1. Kinematics

#### 3.1.1. The AB Doradus Moving Group

Accurate estimation of the age of a single star is notoriously difficult (Soderblom 2010). Stars in clusters and associations have accurate age estimates as the population can be assessed as a whole; the stars can be seen to be coevolving based on their color–magnitude, rotation, and lithium abundance distributions. Planets found in coevolving populations offer much more stringent tests on the temporal evolution of planet properties.

Zuckerman et al. (2004) identified a set of stars within  $\sim 50$  pc comoving with AB Doradus. The star AB Doradus itself is among the closest (15 pc) and most-well-studied young stars. Membership of the group has been revised based on chemo-kinematic analyses of the homogeneity of the stars (da Silva et al. 2009) and updated kinematics from new missions (e.g., Malo et al. 2013; Gagné et al. 2018). Today, dozens of bona fide members define the extent and characteristics of the group, and its age has been estimated to range from 50 Myr (Zuckerman et al. 2004),  $\sim 100$ –120 Myr (Luhman et al. 2005),

$>110$  Myr (Barenfeld et al. 2013), to  $\sim 150$  Myr (Bell et al. 2015).

Figure 8 shows the color–magnitude and space motion of HIP 94235 alongside the AB Doradus moving group and the Pleiades cluster. HIP 94235 shares kinematic properties with the moving group, and has been classified as a bona fide member via Hipparcos (Malo et al. 2013) and Gaia (Gagné et al. 2018; Ujjwal et al. 2020) space motions.

The group has long been linked to Pleiades cluster due to their shared kinematic velocities (Luhman et al. 2005; Ortega et al. 2007). Recent mapping of new low-density moving groups from Gaia (Kounkel & Covey 2019) suggest that the AB Doradus moving group, alongside newly identified Theia 301 and Theia 369 associations, form a long tidal tail streaming away from the Pleiades (Gagné et al. 2021).

Though more distant (130 pc), the Pleiades cluster contains  $\sim 1000$  members, and its age has been more thoroughly investigated than AB Doradus. Estimates converge to  $\sim 120$  Myr via nonrotating isochrones (e.g., Meynet et al. 1993), lithium depletion boundary (e.g., Stauffer et al. 1998; Barrado y Navascués et al. 2004), and 3D rotational isochrones (e.g., Brandt & Huang 2015). The spectroscopic and photometric characteristics of HIP 94235 agree with members of the Pleiades, reaffirming our adopted age of  $\sim 120$  Myr for the system.

#### 3.1.2. An Independent Rotation Sequence for Comoving and Coevolving Stars

The sparsity and spread of the AB Doradus moving group makes it difficult to securely identify true members of the group. The canonical membership list has been evolving with each new chemo-kinematic data set as it was originally defined in Zuckerman et al. (2004). Upcoming Gaia releases with refined radial velocities for fainter distributions of cool stars

**Table 3**  
Properties of HIP 94235

Parameter	Value	Source
<b>Astrometry</b>		
R.A. ...	19:10:57.87	Gaia Collaboration et al. (2021)
decl. ...	−60:16:21.49	Gaia Collaboration et al. (2021)
Parallax (mas) ...	$17.061 \pm 0.037$	Gaia Collaboration et al. (2021)
<b>Proper Motion</b>		
Gaia (2016.1) R.A. Proper Motion ( $\text{mas yr}^{-1}$ ) ...	$11.632 \pm 0.025$	Gaia Collaboration et al. (2021)
Gaia (2016.1) decl. Proper Motion ( $\text{mas yr}^{-1}$ ) ...	$-100.836 \pm 0.025$	Gaia Collaboration et al. (2021)
Hipparcos (1991.1) R.A. Proper Motion ( $\text{mas yr}^{-1}$ ) ...	$12.755 \pm 0.890$	199 (1997)
Hipparcos (1991.4) decl. Proper Motion ( $\text{mas yr}^{-1}$ ) ...	$-99.617 \pm 0.796$	199 (1997)
Hipparcos–Gaia Average R.A. Proper Motion ( $\text{mas yr}^{-1}$ ) ...	$11.509 \pm 0.025$	Brandt (2021)
Hipparcos–Gaia decl. Average Proper Motion ( $\text{mas yr}^{-1}$ ) ...	$-100.628 \pm 0.019$	Brandt (2021)
<b>Photometry</b>		
TESS (mag) ...	$7.758 \pm 0.006$	Stassun et al. (2018)
<i>B</i> (mag) ...	$8.943 \pm 0.027$	Henden et al. (2016)
<i>V</i> (mag) ...	$8.31 \pm 0.03$	Henden et al. (2016)
<i>J</i> (mag) ...	$7.201 \pm 0.023$	Skrutskie et al. (2006)
<i>H</i> (mag) ...	$6.966 \pm 0.023$	Skrutskie et al. (2006)
<i>K</i> (mag) ...	$6.881 \pm 0.027$	Skrutskie et al. (2006)
Gaia (mag) ...	$8.173207 \pm 0.00031$	Gaia Collaboration et al. (2021)
Gaia <sub>BP</sub> (mag) ...	$8.4634 \pm 0.0013$	Gaia Collaboration et al. (2021)
Gaia <sub>RP</sub> (mag) ...	$7.70637 \pm 0.00087$	Gaia Collaboration et al. (2021)
WISE W1 (mag) ...	$6.841 \pm 0.066$	Cutri et al. (2012)
WISE W2 (mag) ...	$6.823 \pm 0.02$	Cutri et al. (2012)
WISE W3 (mag) ...	$6.836 \pm 0.016$	Cutri et al. (2012)
WISE W4 (mag) ...	$6.728 \pm 0.067$	Cutri et al. (2012)
<b>Kinematics and Position</b>		
<i>U</i> ( $\text{km s}^{-1}$ ) ...	$-5.61 \pm 0.34$	Derived
<i>V</i> ( $\text{km s}^{-1}$ ) ...	$-27.03 \pm 0.17$	Derived
<i>W</i> ( $\text{km s}^{-1}$ ) ...	$-11.82 \pm 0.18$	Derived
Distance (pc) ...	$58.54^{+0.08}_{-0.07}$	Derived
<b>Physical Properties</b>		
$M_*$ ( $M_\odot$ ) ...	$1.094^{+0.024}_{-0.007}$	Fitted (Uniform Prior)
$R_*$ ( $R_\odot$ ) ...	$1.08^{+0.11}_{-0.10}$	Fitted (Uniform Prior)
Effective Temperature $T_{\text{eff}}$ (K) ...	$5991 \pm 50$	This paper
Surface Gravity $\log g_*$ (cgs) ...	$4.460 \pm 0.05$	This paper
[m/H] ...	0.0	(Barenfeld et al. 2013)
$v \sin I_*$ ( $\text{km s}^{-1}$ ) ...	$24.4 \pm 1.0$	This paper
$I_*$ (°) ...	$>70$ ( $3\sigma$ )	Calculated as per Masuda & Winn (2020)
Age (Myr) ...	50–150	Zuckerman et al. (2004) Luhman et al. (2005) Bell et al. (2015)
Limb darkening coefficients (TESS) ...	(0.17, 0.41)	Claret (2017)
Limb darkening coefficients (CHEOPS) ...	(0.27, 0.29)	Claret (2017)
<b>Activity indicators</b>		
$P_{\text{rot}}$ (days) ...	$2.24 \pm 0.11$	This paper
Lithium 6708 Å Equivalent Width (Å) ...	$0.1413 \pm 0.0092$	This paper
X-Ray luminosity $\log(L_X/L_{\text{bol}})$	$-3.93 \pm 0.13$	(Boller et al. 2016)

may help redefine groups like AB Doradus and their links with other associations.

To ensure that our age estimation does not hinge on literature classifications of HIP 94235, we also independently search for a comoving population that may confirm its youth.

We follow Tofflemire et al. (2021) and search for stars within 50 pc of HIP 94235 that share its tangential velocity to within  $5 \text{ km s}^{-1}$  using the COMOVE package.<sup>31</sup> In this search, we assume the radial velocity of HIP 94235 for all neighborhood stars. The search returns a set of  $\sim 2000$  stars between  $3 < G < 20$  in magnitude. We then query for TESS MIT QLP light curves, returning 300 matches up to  $T_{\text{mag}} = 13.5$ . We

apply a Lomb–Scargle period search for each light curve, with an upper limit on the rotation period of  $P_{\text{rot}} < 13$ . After manual examination, we find 140 stars that exhibit rotational modulation in their light curves with secure periods.

Figure 9 shows the rotation distribution of these 140 stars relative to the Pleiades. The vast majority of these stars are relatively bright and have well-measured radial velocities from Gaia. We find 21 stars with space motion velocities within  $5 \text{ km s}^{-1}$  of HIP 94235; these are colored in blue for clarity. This population forms a rotation sequence that agrees with HIP 94235. This set of coevolving stars are presented in Table 2.

To estimate the age of the distribution, we fit its color and rotation period with a rotation-age relationship. We select eight F, G, K stars ( $0.1 < B - V < 0.8$ ) within our sample that lie on

<sup>31</sup> <https://github.com/adamkraus/Comove>

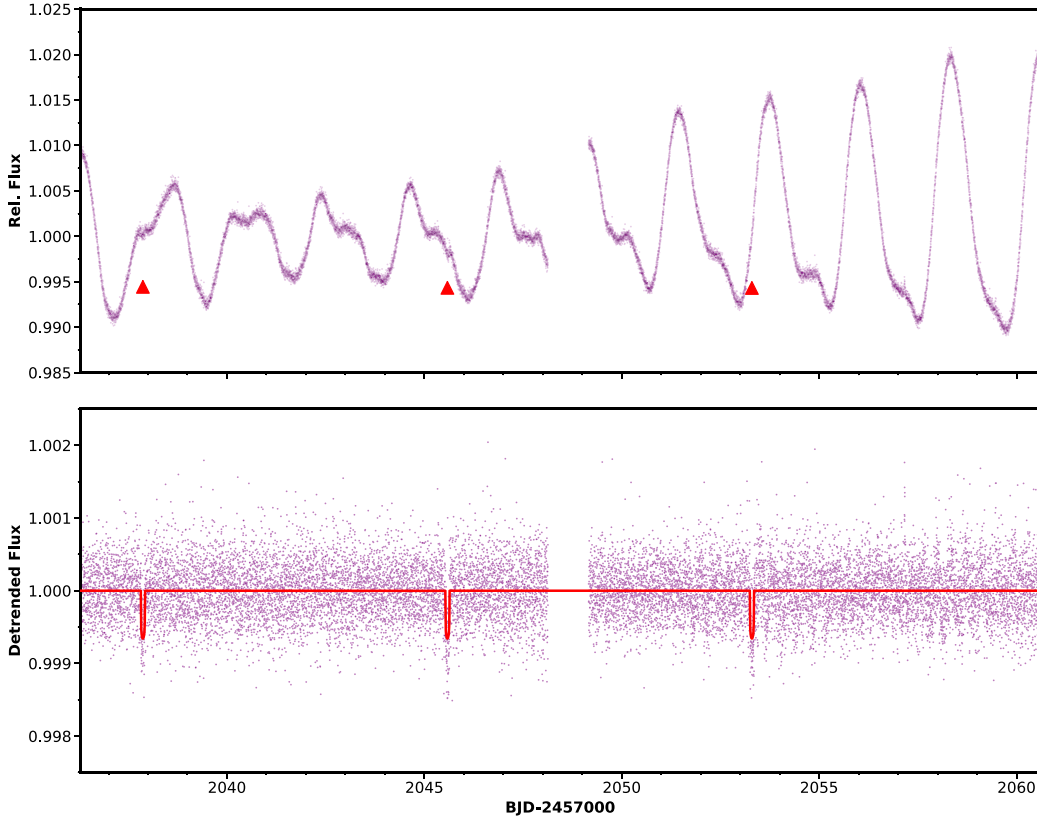


**Figure 2.** Sector 27 2 minutes cadence TESS photometry of the HIP 94235 system. Top: simple Aperture TESS light curve of HIP 94235. The three detected transits of HIP 94235 b are indicated by the arrow marks. Bottom: the custom detrended TESS light curve of HIP 94235 are shown, with the best-fit model overlaid in red.

**Table 4**  
Derived Parameters for HIP 94235 b

Parameter	Joint model	Priors
<b>Fitted Parameters</b>		
$T_0$ (BJD) ...	$2459037.8704^{+0.0011}_{-0.0022}$	Uniform
$P$ (days) ...	$7.713057^{+0.00021}_{-0.00021}$	Uniform
$R_p/R_*$ ...	$0.0253^{+0.00075}_{-0.00059}$	Uniform
$i$ (deg) ...	$87.14^{+0.16}_{-0.17}$	Uniform
$\sqrt{e} \cos \omega$ ...	$0.07^{+0.50}_{-0.54}$	Uniform
$\sqrt{e} \sin \omega$ ...	$0.26^{+0.20}_{-0.27}$	Uniform
$M_p$ ( $M_\oplus$ ) ...	$<379$ ( $3\sigma$ )	Uniform
$\gamma_{\text{MINERVA-Australis 3}}$ ...	$9013^{+58}_{-70}$	Uniform
$\gamma_{\text{MINERVA-Australis 5}}$ ...	$8960^{+123}_{-126}$	Uniform
$\gamma_{\text{MINERVA-Australis 6}}$ ...	$9050^{+88}_{-81}$	Uniform
$\gamma_{\text{CHIRON}}$ ...	$8264^{+31}_{-30}$	Uniform
RV Jitter MINERVA-Australis 3 ...	$80^{+73}_{-56}$	Uniform
RV Jitter MINERVA-Australis 5 ...	$154^{+210}_{-98}$	Uniform
RV Jitter MINERVA-Australis 6 ...	$140^{+113}_{-79}$	Uniform
RV Jitter CHIRON ...	$100^{+35}_{-28}$	Uniform
<b>Inferred parameters</b>		
$e$ ...	$0.32^{+0.20}_{-0.20}$	Derived
$\omega$ (deg) ...	$17^{+67}_{-92}$	Derived
$R_p$ ( $R_\oplus$ ) ...	$3.00^{+0.32}_{-0.28}$	Derived
$a/R_*$ ...	$15.7^{+1.6}_{-1.5}$	Derived
$a$ (AU) ...	$0.07870^{+0.00056}_{-0.00017}$	Derived
Transit duration (days) ...	$0.103^{+0.009}_{-0.018}$	Derived
$K_{\text{rv}}$ ( $\text{m s}^{-1}$ ) ...	$<150$ ( $3\sigma$ )	Derived
$T_{\text{eq}}$ (K) ...	$1060 \pm 50$	Derived

the slow sequence of the rotation sequence, and model their rotation periods with the age–color–rotation relationship from Mamajek & Hillenbrand (2008). The posterior age distribution for these eight stars, and their joint posterior, is shown in Figure 10. We find that the color–rotation distribution of this subsample can be described by the slow sequence with an age of  $118^{+18}_{-16}$  Myr.

We obtained a small number of spectra of this subsample using the Las Cumbres Observatory (Brown et al. 2013) Robotic Echelle Spectrographs (NRES) facilities. The stars that were observed exhibit lithium absorption as expected for their youth. The lithium  $6708 \text{ \AA}$  equivalent width has been noted in Table 2 where available. Future works examining the lithium absorption of this subsample may yield a lithium depletion boundary to confirm this age estimate.

Of these 21 comoving stars, only one is a canonical member of AB Doradus (Gagné et al. 2018). It is likely that the AB Doradus moving group itself is dispersed and ill defined, and our subset of comoving and potentially coevolving stars form part of the extended AB Doradus group.

### 3.2. X-Rays

The rapid rotation in young stars leads to increased chromospheric activity. As a result, young stars often exhibit higher X-ray and UV emissions than their slowly rotating older counterparts. HIP 94235 is cataloged in the Second ROSAT All-sky Bright Source Catalog (Boller et al. 2016). HIP 94235 matches with 2RXS J191057.9–601611, with a count rate of  $0.1766 \pm 0.0425$  counts  $\text{s}^{-1}$  and a hardness ratio of  $-0.124 \pm 0.176$ . Using the calibration from Fleming et al. (1995), we find an X-ray luminosity for HIP 94235 of  $\log(L_X/L_{\text{bol}}) = -3.93 \pm 0.13$ .

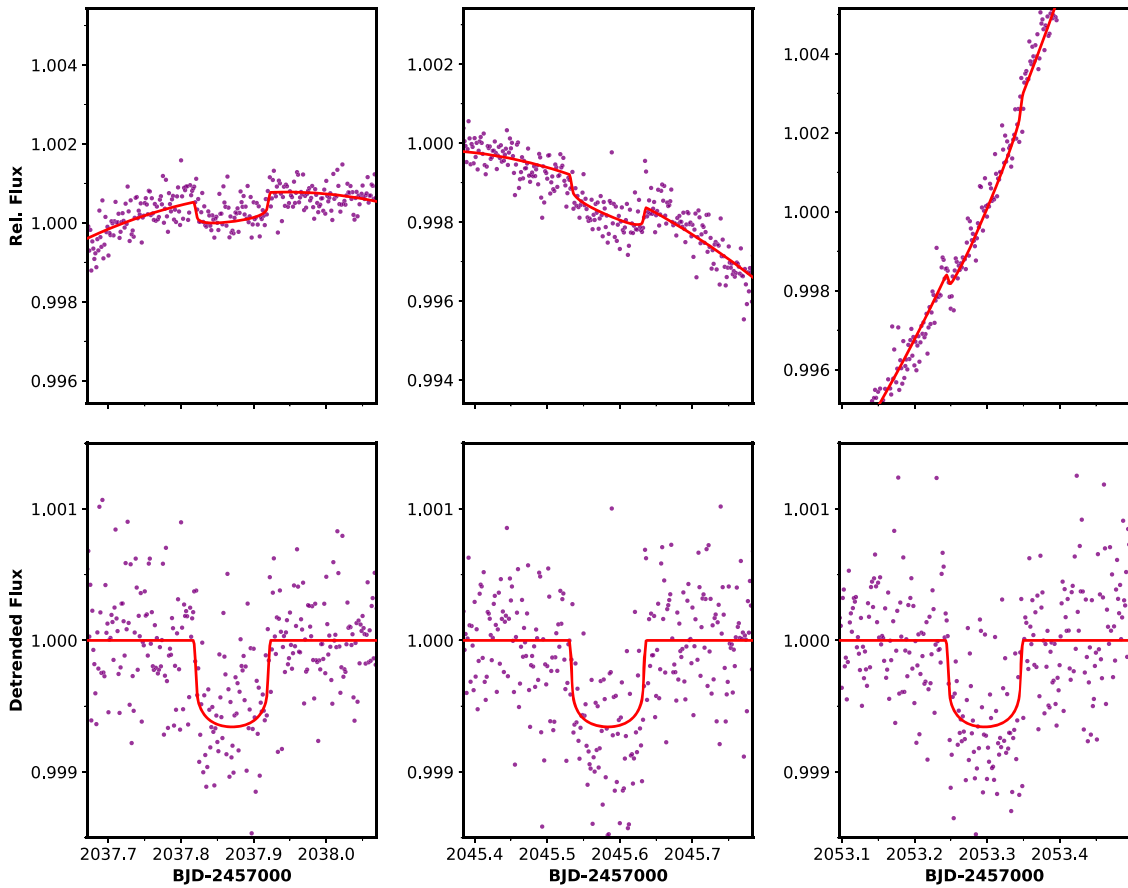


**Figure 3.** Individual transits of HIP 94235 b from TESS Sector 27. The top row shows the transits pre-detrending, the bottom row shows the same transits post-detrending. The best-fit transit model is overlaid in red.

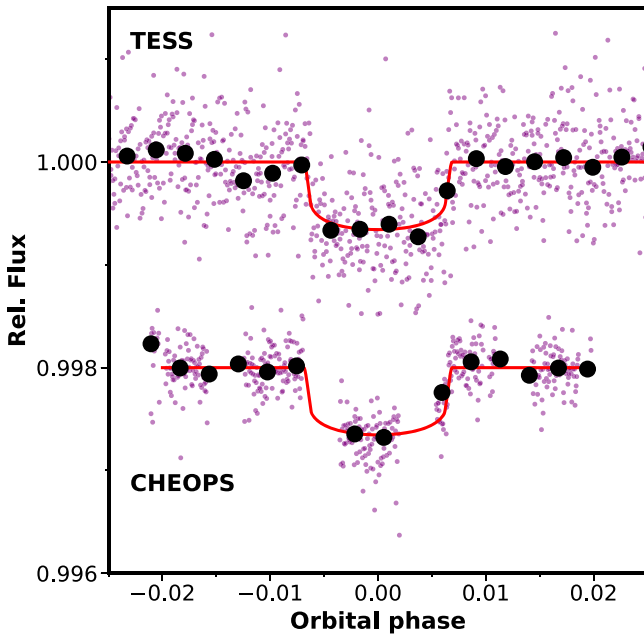


**Figure 4.** Phase-folded transit light curves from TESS (Top) and CHEOPS (Bottom). The black points show the data set binned at 30 minutes intervals. The red lines show the respective models from our global analysis.

The strength of the X-ray activity can help yield a qualitative age estimate for a single star. We adopt Equation (A3) from Mamajek & Hillenbrand (2008) to find an approximate age of

50–130 Myr ( $1\sigma$ ) for HIP 94235 from its X-ray luminosity, consistent with the expected age of the AB Doradus group.

### 3.3. Lithium

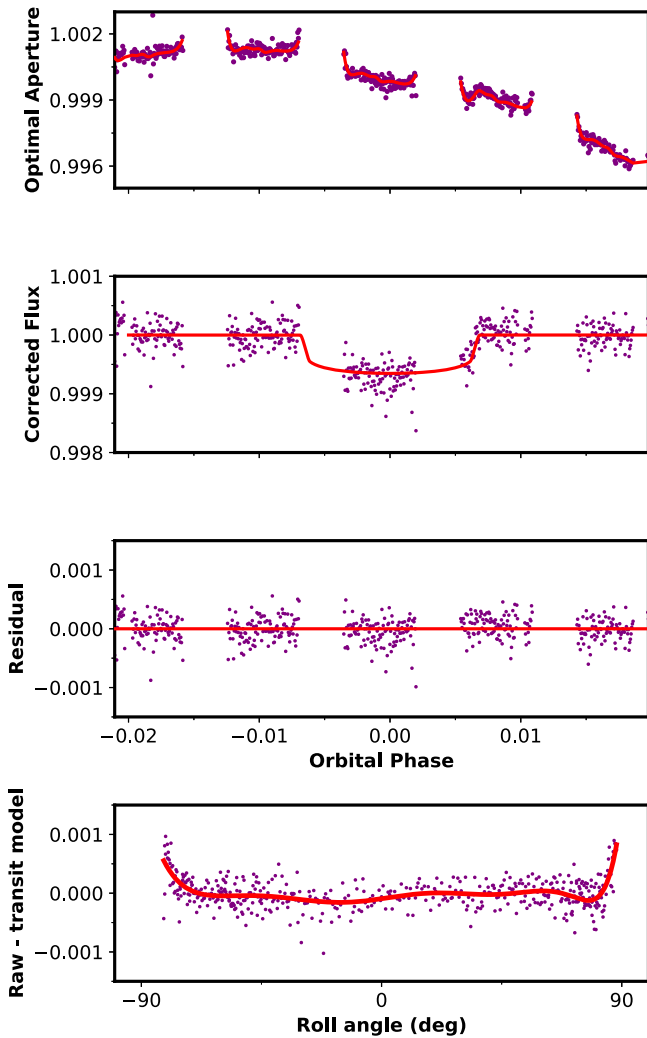
Stars undergo lithium depletion during their main-sequence evolution. Lithium is depleted during proton collisions in the cores of stars. Convective mixing between the envelope and the core leads to a gradual depletion of lithium absorption in the observed spectra of Sun-like stars. As such, the lithium abundance of a star can be a tracer for its youth, though direct age estimates from the lithium absorption strength is only qualitative, as is the case for any age indicator when interpreting single stars. Our CHIRON spectra of HIP 94235 reveal significant absorption about the 6708 Å Li doublet. We model the doublet and the nearby Fe I line simultaneously, measuring a Li equivalent width of  $0.1413 \pm 0.0092$  Å for HIP 94235.

Figure 11 compares the lithium 6708 Å equivalent width against distributions from known AB Doradus members (da Silva et al. 2009), Pleiades, and Praesepe clusters (Quinn et al. 2012, 2014; Zhou et al. 2021). HIP 94235 is consistent with that of other known members of AB Doradus and Pleiades, and exhibits convincingly stronger lithium absorption than members of the 600 Myr Praesepe cluster, in agreement with a 120 Myr age estimate.

### 3.4. Rotation

The TESS observations show that HIP 94235 exhibits significant photometric variability at the 2% level, consistent





**Figure 5.** Transit of HIP 94235 b as captured by CHEOPS on 2021 August 19 over five CHEOPS orbits. The first panel shows the pre-detrending light curve extracted at an optimal aperture of 31 pixels. The large-scale smooth variation is induced by the spot modulation of the target star and is accounted for in our model via a fourth-order polynomial. Orbital-timescale variations are also present, and are accounted for via a fifth-order polynomial fit between the spacecraft roll angle and the light-curve residuals, after subtraction of the transit, spot modulation signal, and instrumental systematics models. The second panel shows the detrended CHEOPS light curve. The third panel shows the residuals after subtraction of the transit, spot modulation signal, and instrumental systematics models. The fourth panel shows the correlation between the light curve, after removal of the transit and spot modulation signals, and the spacecraft roll angle, with the best-fit model overlaid.

with the semi-periodic signature of spot modulation. Figure 12 shows the periodicity of HIP 94235 via a Lomb–Scargle periodogram, with a peak rotation period of  $2.24 \pm 0.11$  days. We adopt the width of the rotational peak of the periodogram as the uncertainty on the measured period. The rotational modulation is clear in phase-folded light curve in the right panel of Figure 12, and the evolution of starspots over successive rotations can also be seen. Additionally, we modeled the light curve via a stochastically driven damped harmonic oscillator through a Gaussian process using the CELERITE package (Foreman-Mackey et al. 2017). Modeling the posterior via a Markov chain through EMCEE (Foreman-Mackey et al. 2013), we found a posterior distribution for the frequency term  $\log \omega_0$  to be  $-0.791_{-0.045}^{+0.047}$ , corresponding to a period of  $2.20 \pm 0.10$  days.

Figure 11 shows the rotation periods of AB Doradus, as well as the Pleiades and Praesepe cluster members. We adopt the membership list for AB Doradus from Gagné et al. (2018), and derived rotation periods for stars with available TESS light curves from the MIT FFI QLP library (Huang et al. 2020b) for stars with available light curves. Rotation periods are measured via a Lomb–Scargle period search and down-selected by hand to remove stars that do not show unambiguous rotational signatures. By-hand corrections of period aliases were also applied. Of the 66 members listed in Gagné et al. (2018), 55 were bright enough and had accessible TESS QLP light curves, and 37 yielded convincing detections of a rotation signal. Rotation periods for Pleiades members were adopted from Rebull et al. (2016), and for Praesepe from Rebull et al. (2017). The rotation of HIP 94235 agrees with the Pleiades and AB Doradus distribution, in agreement with its kinematic age estimates.

#### 4. Global Model

To best estimate the stellar and planetary properties of the HIP 94235 system, we perform a global modeling incorporating the TESS and CHEOPS transits, radial velocities, and photometric and spectroscopic properties of HIP 94235.

The transit models were computed as per Mandel & Agol (2002), implemented via BATMAN (Kreidberg 2015). The free parameters for this model are the stellar mass and radius, the time of transit center  $T_0$ , the orbital period  $P$ , the planetary radius ratio  $R_p/R_*$ , and the eccentricity parameters  $\sqrt{e} \cos \omega$  and  $\sqrt{e} \sin \omega$ , where  $e$  is the eccentricity and  $\omega$  is the longitude of periastron.

We model the CHEOPS transit and its associated stellar variability and instrumental characteristics simultaneously to the global modeling. The transit model is computed as per Mandel & Agol (2002). The hour-long rotational modulation signal is modeled via a fourth-degree polynomial with respect to time. The correlation between the light curve and the spacecraft motion is modeled via a fifth-degree polynomial against the roll angle. Figure 5 shows the CHEOPS light curve before and after the removal of the best-fit stellar variability and instrumental model.

The out-of-transit Keplerian radial velocity was modeled with additional parameters describing the systemic velocity  $\gamma$ , planetary mass  $M_p$ , and a jitter term for each instrument.

The stellar mass and radius were modeled using the Modules for Experiments in Stellar Astrophysics Isochrones and Stellar Tracks (MIST; Dotter 2016), and constrained by their photometric magnitudes and parallax priors from Gaia  $G$ ,  $B_p$ ,  $R_p$  (Gaia Collaboration et al. 2018), the Hipparcos TYCHO  $B$  and  $V$  bands (Perryman et al. 1997), the Two Micron All Sky Survey (2MASS)  $J$ ,  $H$ , and  $K_s$  bands (Skrutskie et al. 2006). Additionally, the age was restricted to be  $120 \pm 50$  Myr as per the age of the AB Dor moving group, and the limb darkening coefficients were fixed to theoretically interpolated values (Claret & Bloemen 2011; Claret 2017). All other parameters were assigned uniform priors with physically motivated boundaries.

The modeling was performed simultaneously for all parameters using Monte Carlo Markov Chain (MCMC) analysis, making use of the emcee package (Foreman-Mackey et al. 2013). Results are listed in Tables 3 and 4, the best-fit light-curve model is shown in Figure 2, and the best-fit radial velocity model is shown in Figure 7. The spectral energy distribution of HIP 94235 is shown in Figure 13, along with the

**Table 5**  
Diffraction Limited Measurements of HIP 94235 B

Instrument	Epoch	Separation (mas)	Position Angle (°)	$\Delta m$ (mag)	Reference
VLT-NaCo	2010 July 30	$506 \pm 7$	$150.6 \pm 0.8$	$3.8 \pm 0.3$ ( <i>H</i> band)	Chauvin et al. (2015), Desidera et al. (2015)
Gemini-Zorro	2021 July 23	$596 \pm 5$	$162.87 \pm 0.48$	5.84 (832 nm)	This Work
Gemini-Zorro	2021 October 22	$600 \pm 8$	$161.73 \pm 0.75$	5.31 (832 nm)	This Work

**Table 6**  
Orbital Parameters of HIP 94235 B

Parameter	Median $\pm 1\sigma$	Mode	Priors
<b>Informed Priors</b>			
Parallax (mas) ...	$17.061 \pm 0.037$	–	Gaussian
$M_A (M_\odot)$ ...	$1.094 \pm 0.05$	–	Gaussian
$M_B (M_\odot)$ ...	$0.26 \pm 0.04$	–	Gaussian
<b>Fitted Parameters</b>			
$a$ (AU) ...	$56^{+9}_{-7}$	54	Log-uniform
$\sqrt{e} \sin \omega$ ...	$0.35^{+0.14}_{-0.19}$	0.40	Uniform
$\sqrt{e} \cos \omega$ ...	$0.20^{+0.48}_{-0.34}$	0.48	Uniform
Mean anomaly at BJD = 2457000 (deg) ...	$170^{+110}_{-80}$	130	Uniform
$i$ (deg) ...	$67.8^{+2.7}_{-2.9}$	67.4	$\sin i$
$\Omega$ (deg) ...	$20^{+11}_{-7}$	18	Uniform
Barycentric R.A. proper motion (mas yr <sup>-1</sup> ) ...	$10.50 \pm 0.24$	10.46	Uniform
Barycentric decl. proper motion (mas yr <sup>-1</sup> ) ...	$-102.99 \pm 0.35$	102.91	Uniform
<b>Derived Parameters</b>			
$P$ (years) ...	$365^{+92}_{-69}$	362	Derived
$e$ ...	$0.25^{+0.22}_{-0.14}$	0.19	Derived
$\omega$ (deg) ...	$300^{+30}_{-80}$	320	Derived
Periastron distance (AU) ...	$43^{+11}_{-15}$	47	Derived
Time of periastron (years CE) ...	$2184^{+107}_{-74}$	2164	Derived

template ATLAS9 model spectrum (Castelli & Kurucz 2004) computed at the best-fit stellar parameters of HIP 94235. We note that the mid-infrared Wide-field Infrared Survey Explorer (WISE) magnitudes show no excess that might be indicative of a remnant debris disk around the young star.

## 5. HIP 94235 B: A 60 au M-dwarf Companion

Diffraction limited observations revealed a bound M-dwarf companion to HIP 94235. The companion was identified in speckle imaging observations of HIP 94235 during the candidate vetting process, and also identified from archival adaptive optics observations searching for wide Jovian companions to young stars 11 yr prior. We describe the observations below and perform compute astrometric orbital solutions for HIP 94235 B.

We obtained high-contrast imaging at 562 nm and 832 nm with the Zorro speckle imager on the 8 m Gemini South Observatory on 2021 July 23 and 2021 October 22, which revealed a faint stellar companion to HIP 94235. Zorro is a dual-channel speckle imager with a pixel scale of  $0''.01 \text{ pixel}^{-1}$  and an approximate FWHM of  $0''.02$ . Data reduction and analysis were performed as per Howell et al. (2011) and Howell et al. (2016). Figure 14 shows the Zorro image at 562 nm and 832 nm of HIP 94235 on 2021 October 22. The

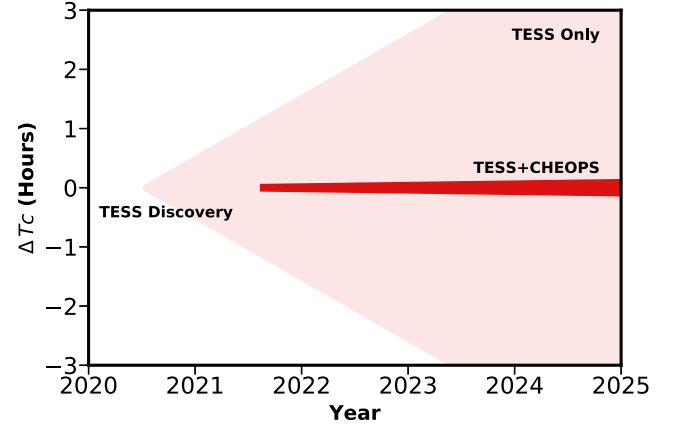


**Figure 6.** Transit timing uncertainty for HIP 94235 b with and without follow-up CHEOPS observations. With only the single sector of TESS observations, the timing uncertainty erodes by  $\sim 1 \text{ hr yr}^{-1}$ , quickly making targeted transit follow-up difficult. The CHEOPS transit allowed the transit ephemeris to be preserved.

832 nm observation achieved a contrast ratio of  $\Delta m = 6.68$  at  $0''.5$  separation. A companion of  $\Delta m = 5.3$  was identified at a separation of  $0''.6$  in the red band. No companions with contrasts brighter than  $\Delta m = 4.7$  were detected in the blue arm. Observations from 2021 July 23 also identified the same companion in the 832 nm observations, though the blue arm was not functional at the time.

Adaptive optics imaging of HIP 94235 was also carried out as part of a large program to characterize the occurrence rates of giant planets at large separations by Chauvin et al. (2015). These observations, using the NaCo high-contrast adaptive optics (AO) imager on VLT-UT4, were obtained on 2010-07-30. They revealed the stellar companion at a separation of  $0''.5$  with a contrast of  $\Delta H = 3.8 \pm 0.3$ . The positional information from the diffraction limited imaging observations are listed in Table 5.

Based on the Gaia and Hipparcos proper motions measurements, the accumulated motion of HIP 94235 over the 11 yr interval is  $1''.1$ . In contrast, the relative motion between the imaged companion and the target star is  $0''.1$ , which strongly suggests the pair is a bound stellar binary with a projected separation of 31 au. We henceforth refer to this companion as HIP 94235 B.

To determine the approximate properties of HIP 94235 B, we adopt the 100 Myr MIST isochrones (Choi et al. 2016) to model its 832 nm and *H*-band magnitudes. We approximate the 832 nm band with the *I*-band magnitudes from MIST, and adopt magnitudes for the companion of  $I = 10.76 \pm 0.3$  and  $H = 13.05 \pm 0.4$ . We adopt a fixed metallicity of  $[M/H] = 0$  as per that for the AB Doradus moving group (da Silva et al. 2009) and adopt a strong Gaussian prior for the distance to HIP 94235 B as per its Gaia parallax. We find the companion is an

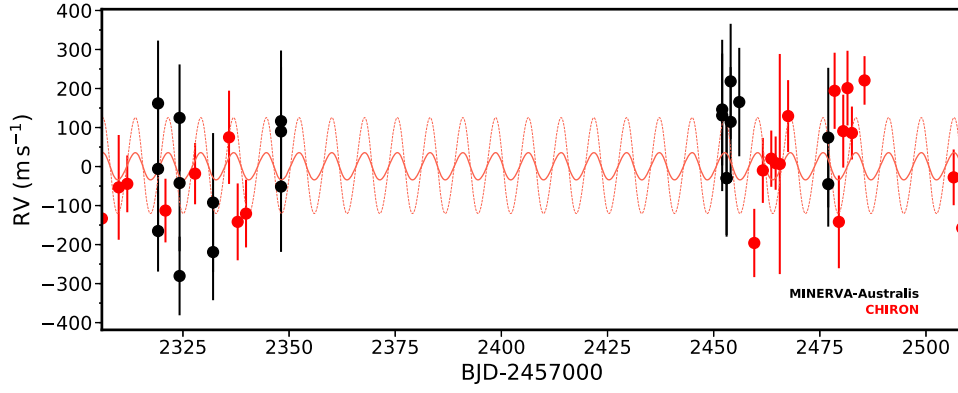


**Figure 7.** Radial velocities for HIP 94235 from CHIRON (red) and MINERVA-Australis (black), with error bars representing the quadrature addition of the observational uncertainties and the best-fit jitter. No orbital variations were detected, as expected for a small planet about an active, rapidly rotating star. The velocity orbit upper limits at  $1\sigma = 0.35 M_{\text{jup}}$  and  $3\sigma = 1.27 M_{\text{jup}}$  are shown in the solid and dashed red curves, respectively.

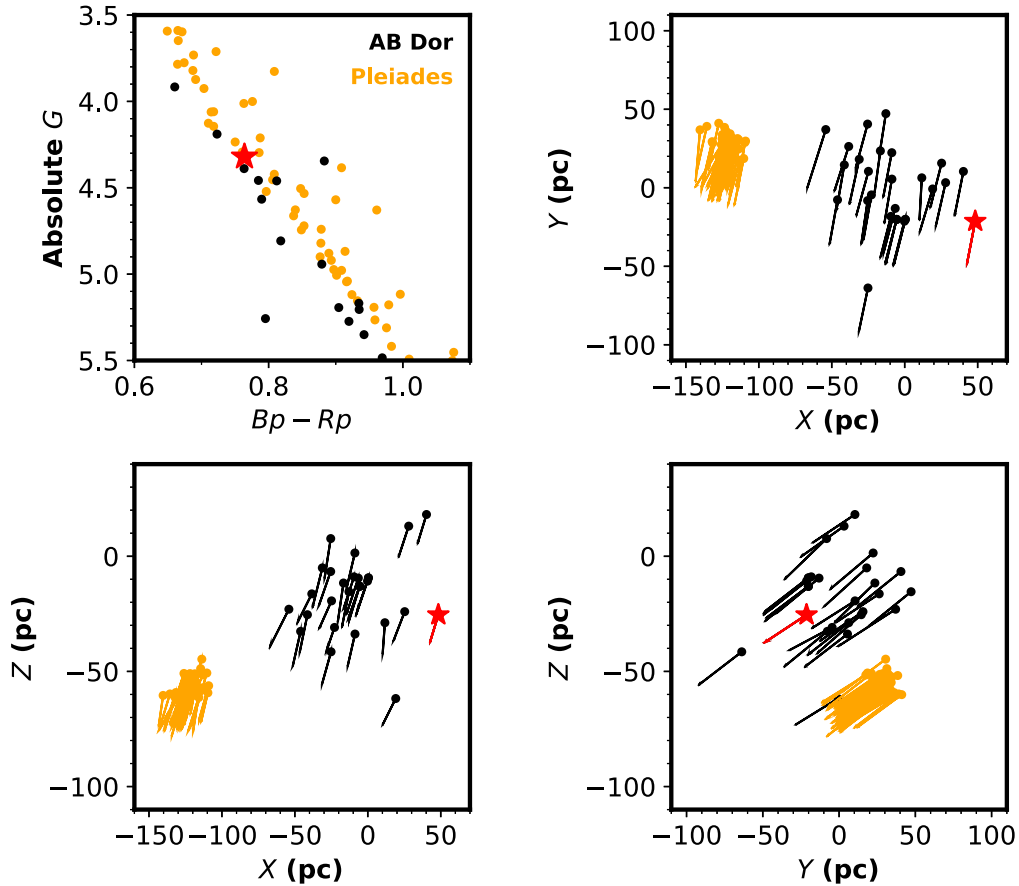


**Figure 8.** HIP 94235 can be placed kinematically in the  $\sim 120$  Myr old AB Doradus moving group. The figure shows the photometric and space motion properties of stars in AB Doradus and Pleiades from Gagné et al. (2018). Both groups have ages of  $\sim 120$  Myr, and are thought to be comoving (Luhman et al. 2005; Ortega et al. 2007; Kounkel & Covey 2019). The top left panel shows the Gaia color-magnitude diagram for the two clusters. The remaining panels show the galactic positions  $X$ ,  $Y$ ,  $Z$  and motions  $u$ ,  $v$ ,  $w$  of the selection. HIP 94235 is marked by the red star in all panels. The local standard of rest has not been corrected for in the velocities.

M-dwarf of mass  $0.26 \pm 0.04 M_{\odot}$  and radius  $0.31 \pm 0.03 R_{\odot}$ . The companion is incapable of hosting the transiting companion responsible for the planetary transit signal detected in TESS. To check if this companion is capable of being the source of the transit signal, we deblend and refit for the transit about the M-dwarf companion. We find a best-fit radius ratio of  $R_2/R_1 = 0.46 \pm 0.01$  for such a system, with a V-shaped transit that is incompatible with the observed light curve. A model

comparison yields a Bayesian information criterion difference of  $\Delta\text{BIC} = 65.9$  between the best-fit model of a transit about the companion M-dwarf and that of our nominal planetary transit scenario. We therefore rule out the companion being the source of the observed transit signal.

Although the available imaging detections cover only a small part of the orbital arc of HIP 94235 B, it is possible in principle that the binary orbit could be constrained. Several authors (e.g.,

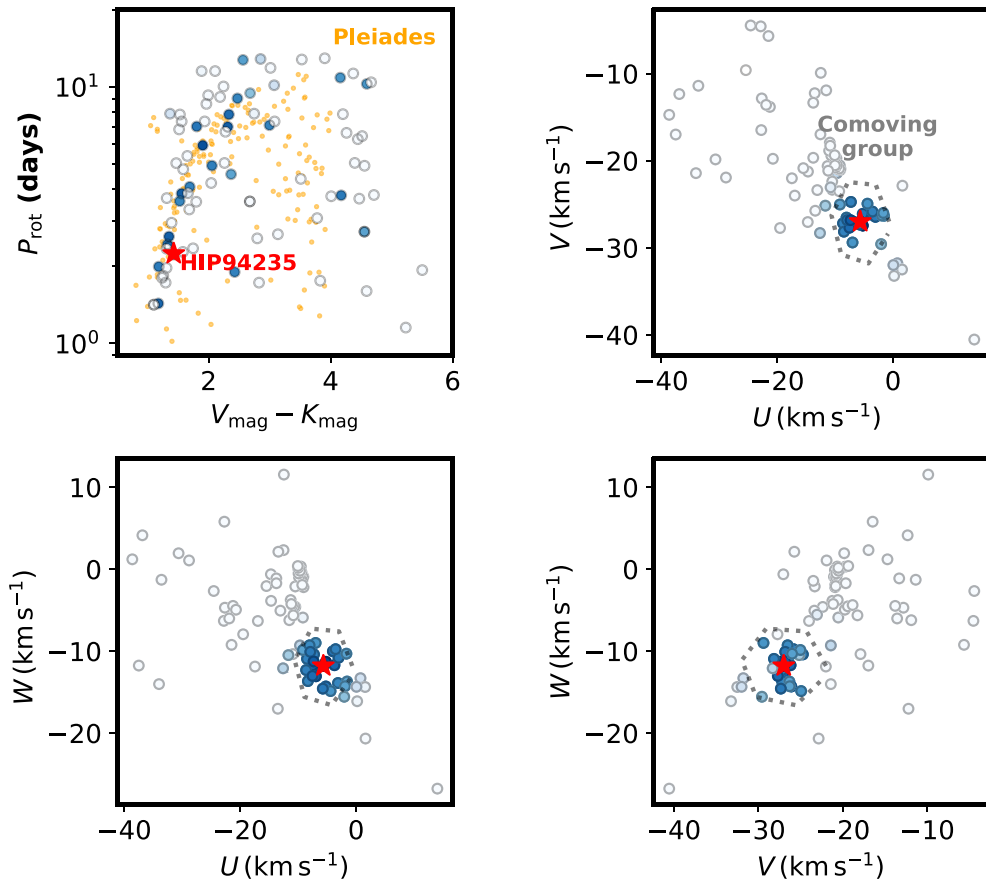


**Figure 9.** Distribution of stars sharing tangential velocities of HIP 94235 identified in our neighborhood search. Top left: We find 140 stars to exhibit clear rotational signatures in their TESS light curves. The blue points are located within  $5 \text{ km s}^{-1}$  of HIP 94235 in  $U$ ,  $V$ , and  $W$ . These blue points form rotation sequence that agrees with the expected age of HIP 94235 at 120 Myr. The Pleiades sequence from Rebull et al. (2016) is shown in yellow. The remaining panels show the  $U$ ,  $V$ , and  $W$  velocity distribution of the tangentially comoving stars. A clear group can be found around HIP 94235 and is marked out by the  $5 \text{ km s}^{-1}$  boundary in gray.

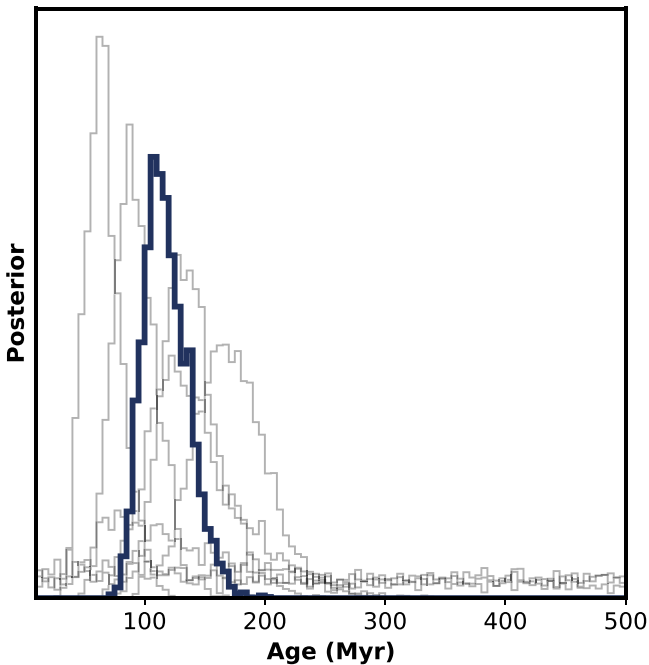


**Figure 10.** Age posterior of a subsample of F, G, K stars that are comoving with HIP 94235. We fit the age relationship from Mamajek & Hillenbrand (2008) to this population. The age posterior of each individual star is shown in gray, and the joint posterior in blue. We find a best-fit age of  $118_{-16}^{+18}$  Myr to the distribution.

Brandt 2018; Calissendorff & Janson 2018; Snellen & Brown 2018; Kervella et al. 2019) have demonstrated that it is possible to combine proper motion measurements from Gaia and Hipparcos to produce long-timescale astrometric data that can be used to detect the reflex orbital motion of orbiting companions. Brandt et al. (2019) extended this technique further by jointly fitting Hipparcos–Gaia astrometry with radial velocities and relative astrometry from direct imaging, and found that the orbits of massive companions can be precisely constrained even when the orbital periods are much longer than the observational duration. This method has been profitably applied to many further systems; Bowler et al. (2021), for example, were able to extract precise orbital parameters and masses for two white dwarfs with orbital periods in excess of  $\gtrsim 200$  yr despite possessing no more than  $\sim 30$  yr of observational data in both cases.

Inspection the Hipparcos–Gaia Catalog of Accelerations (Brandt 2021) shows that HIP 94235 displays a statistically significant astrometric acceleration of  $0.24 \text{ mas yr}^{-1}$  ( $\chi^2 = 58.5$ ) between the Gaia and Hipparcos–Gaia proper motions, equivalent to a drift in the stellar tangential velocity of  $\approx 70 \text{ m s}^{-1}$ , which can plausibly be attributed to HIP 94235 B. This motivates us to attempt an orbital fit for HIP 94235 B based on the available data.

To initialize our model we first used `orbitize!` (Blunt et al. 2020) to fit the relative astrometry of HIP 94235 B assuming a total system mass of  $1.09 + 0.26 = 1.35 M_{\odot}$ . `orbitize!` makes use of the orbits for the impatient (OFTI)

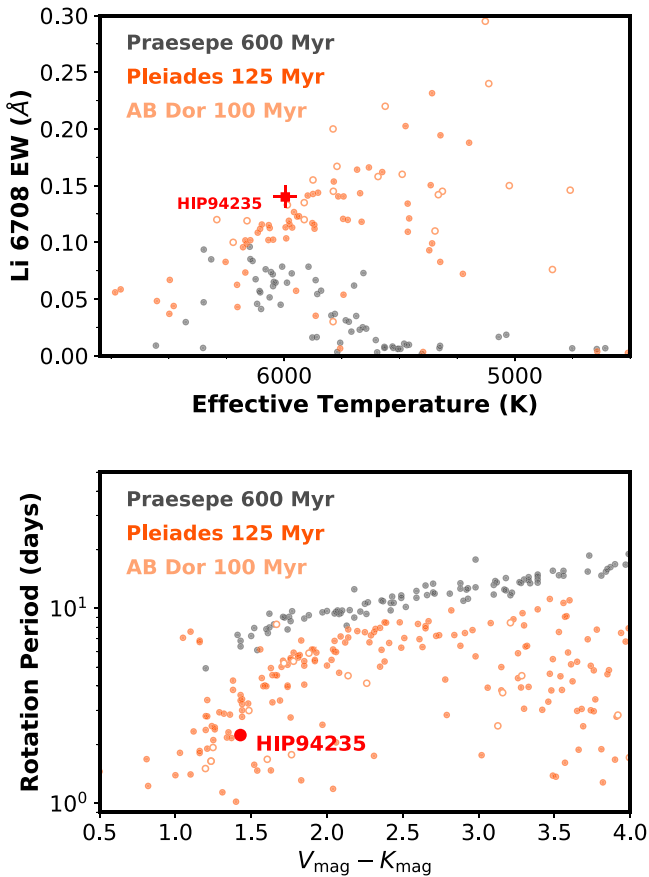


**Figure 11.** Age indicators of HIP 94235 are consistent with that from AB Doradus and Pleiades members. AB Doradus members are shown in open orange circles, Pleiades members in closed orange circles, and Praesepe members in gray. The top panel shows the distribution of Li 6708 Å doublet equivalent widths for AB Doradus (da Silva et al. 2009), Pleiades, and Praesepe members (Quinn et al. 2012, 2014; Zhou et al. 2021). Bottom panel shows the distribution of rotation periods for the same set of stars.

Bayesian sampling method (Blunt et al. 2017) that is well-suited to fitting the orbits of directly detected companions with orbital periods much longer than the observational span such as HIP 94235 B. Next we extracted the posteriors from the *orbitize!* fit and calculated the corresponding  $\chi^2$  value for a fit to the Hipparcos–Gaia astrometry for each set of orbital parameters assuming stellar masses of  $M_A = 1.09 M_\odot$ ,  $M_B = 0.26 M_\odot$ . This allowed us to identify a tightly constrained initial parameter space for most orbital parameters.

To model the orbit of HIP 94235 B, we run a joint fit to the astrometry based on that of Brandt et al. (2019). For modeling the Hipparcos–Gaia astrometry we use the equations described in Venner et al. (2021b), while the corresponding expressions for the relative astrometry can be found in Pourbaix (1998). As in Venner et al. (2021a, 2021b), we resample the Hipparcos and Gaia proper motions using the observational epochs recorded in the Hipparcos Intermediate Astrometric Data for the former and the Gaia Observation Forecast Tool<sup>32</sup> for the latter. To explore the model parameter space we use the differential evolution MCMC sampler *edmc*<sup>33</sup> (Vanderburg 2021).

A total of 11 parameters are used for the model: the system parallax  $\varpi$ , the primary mass  $M_A$ , the secondary mass  $M_B$ , the

semimajor axis  $a$ , the eccentricity  $e$ , and argument of periastron  $\omega$  parameterized as  $\sqrt{e} \sin \omega$  and  $\sqrt{e} \cos \omega$ , the mean anomaly at an arbitrary reference epoch  $\text{BJD} = 2457000$ , the orbital inclination  $i$ , the longitude of node  $\Omega$ , and finally two terms for the proper motion of the system barycenter.

The radial velocity trend generated by HIP 94235 B is too small to be detected in the available data so we do not make use of radial velocity (RV) data in the joint fit. The lack of radial velocity information in the fit results in the classical 180° degeneracy in the longitude of node  $\Omega$  and argument of periastron  $\omega$ ; following convention we report the solution with  $\Omega$  in the range  $[0, 180]$  deg. The argument of periastron used in our model is that of the primary’s orbit rather than that of the companion.

Of the 11 parameters used in the joint model, the parallax  $\varpi$  was assigned a Gaussian prior of  $17.061 \pm 0.037$  mas based on the Gaia EDR3 astrometric solution while the primary mass  $M_A$  was given a Gaussian prior of  $1.094 \pm 0.05 M_\odot$ , with an inflated uncertainty as compared to the value in Table 3 to avoid unduly biasing the model. Initial trials of the orbital fit were run without informed priors on the secondary mass  $M_B$  however these runs tended to produce results skewed toward implausibly small values for this parameter ( $M_B < 0.1 M_\odot$ ), which in turn resulted in excessively broad distributions in the orbital parameters. It was therefore deemed prudent to adopt an informed prior of  $M_B = 0.26 \pm 0.04 M_\odot$  for the final model.

The results of our joint model for the orbit of HIP 94235 B are presented in Table 6. Despite the span of observations being much shorter than the orbital period of the binary, we are able to robustly constrain most orbital parameters. We measure a semimajor axis of  $a = 56_{-7}^{+9}$  au for HIP 94235 B, approximately  $\approx 80\%$  larger than the projected separation, corresponding to an orbital period of  $365_{-69}^{+92}$  yr. Our model shows a preference for relatively low orbital eccentricities ( $0.25_{-0.14}^{+0.22}$ ,  $e < 0.61$  at 95% confidence), resulting in a periastron separation of  $43_{-15}^{+11}$  au for the binary. We obtain a tightly constrained orbital inclination of  $67.8_{-2.9}^{+2.7}$  and a precise longitude of node of  $20_{-7}^{+11}$  degrees, while our measurements of  $\omega$  and the time of periastron for HIP 94235 B are comparatively imprecise ( $300_{-80}^{+30}$  deg,  $2184_{-74}^{+107}$  CE).

Our fit to the astrometric data is shown in Figures 15 and 16. In the fit to the absolute astrometry it can be observed that the Hipparcos proper motion measurement is too imprecise to significantly detect the astrometric signal. Conversely, the Gaia and averaged Hipparcos–Gaia proper motions are so precise that their uncertainties are not visible in the figure, and it is these measurements that drive the detection of the astrometric reflex signal of HIP 94235 B. The importance of the  $>10$  yr time span of relative astrometry is evident from Figures 15 and 16, as were it not for the detection of HIP 94235 B in an archival NaCo observation in 2010 it would not be possible to derive such strong constraints on the binary orbit.

We note that the astrometric orbit solution is dependent on the priors we adopt for the system. For example, when the mass prior for HIP 94235 B is removed, the orbital semimajor axis becomes degenerate with eccentricity. As such, future diffraction limited observations remain important in validating and refining the orbital parameters of the system.

Based on our results, we predict the magnitude of the radial velocity trend on HIP 94235 generated by HIP 94235 B to be  $9.6 \pm 1.3 \text{ m s}^{-1} \text{ yr}^{-1}$ . This trend is not detectable in our RV data, but it is possible that future high-precision radial velocity

<sup>32</sup> <https://gaia.esac.esa.int/gost/>

<sup>33</sup> <https://github.com/avanderburg/edmc>

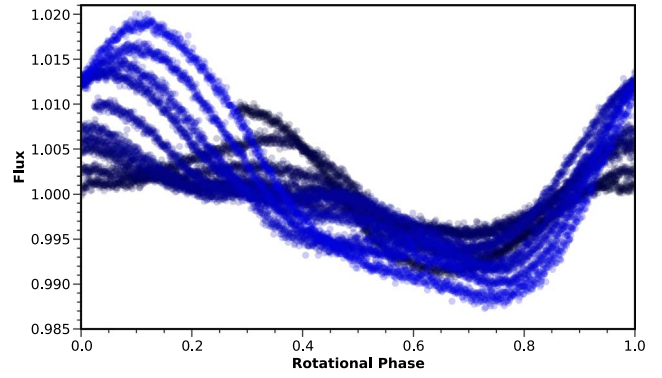
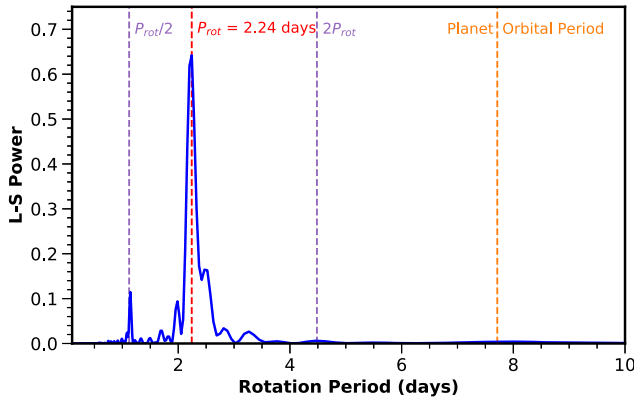


**Figure 12.** Left: Lomb–Scargle periodogram of the HIP 94235 from its TESS light curve. The red dashed line denotes the adopted rotation period, while the dotted purple lines denote the aliases at  $P/2$  and  $2P$ . The orbital period of the planet is marked in orange. Right: Phase-folded TESS light curve, with a color gradient applied such that later periods are a lighter blue.

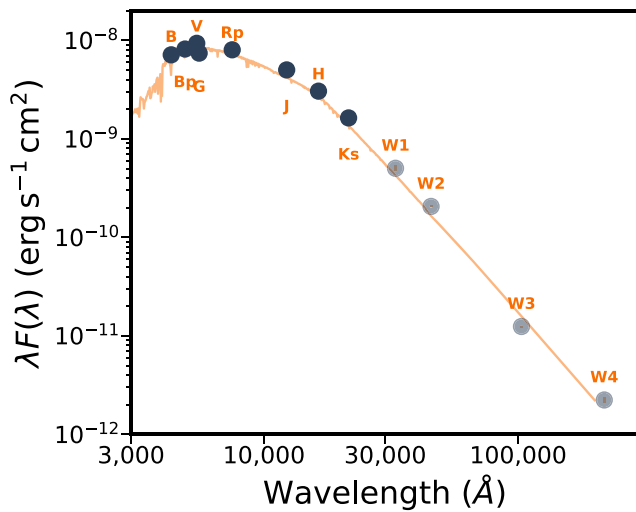


**Figure 13.** Spectral energy distribution of HIP 94235. Magnitudes from Tycho  $B$ ,  $V$ , Gaia  $B_p$ ,  $G$ ,  $R_p$ , 2MASS  $J$ ,  $H$ ,  $K_s$ , and WISE  $W1$ ,  $W2$ ,  $W3$ ,  $W4$  are plotted. We note that WISE  $W1$ ,  $W2$ ,  $W3$ ,  $W4$  were not used in the global modeling, and are marked by a lighter color compared to the bluer bands. The template spectrum from ATLAS9 model atmospheres (Castelli & Kurucz 2004) is plotted for reference.

measurements will be able to detect this acceleration. If so, the radial velocity information could then be used to improve the constraints on the orbit of HIP 94235 B.

## 6. Summary and Discussion

We report the discovery and statistical validation of a mini-Neptune around a bright young Sun-like star. HIP 94235 b is a  $3.00^{+0.32}_{-0.28} R_{\oplus}$  planet in a 7.7 day period orbit around its  $V_{\text{mag}} = 8.31$  host star. Based on its kinematics, HIP 94235 can be placed in the AB Doradus moving group, with an age of  $\sim 120$  Myr. The kinematics age is in agreement with that expected from the stellar rotation rate, lithium abundance, and X-ray emission intensity.

The 600 ppm transits of HIP 94235 b were identified at a signal-to-noise of 9.7 from TESS Extended Mission Section 27 observations. However, the two-day periodicity 2% stellar variability led to the planetary signal slipping through the TESS official planet selection processes. The detection of HIP 94235 b demonstrated the necessity of a dedicated search for planets around noisy, active young stars. Confirmation of transits came

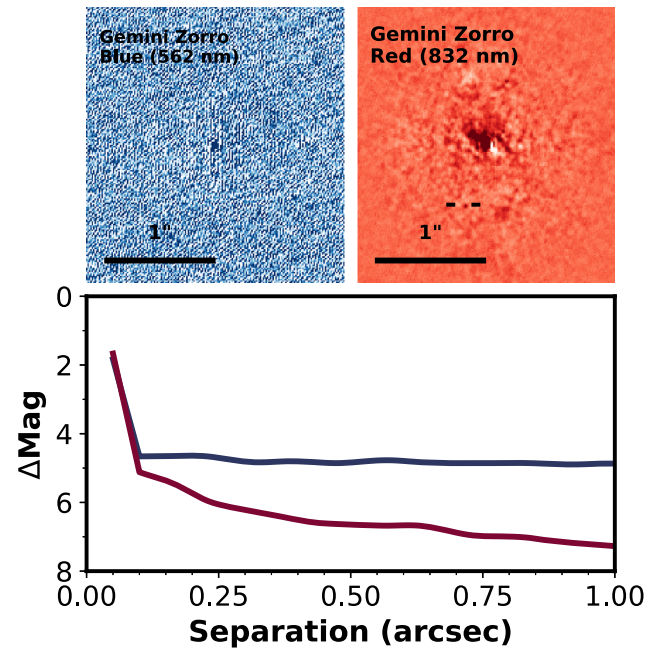
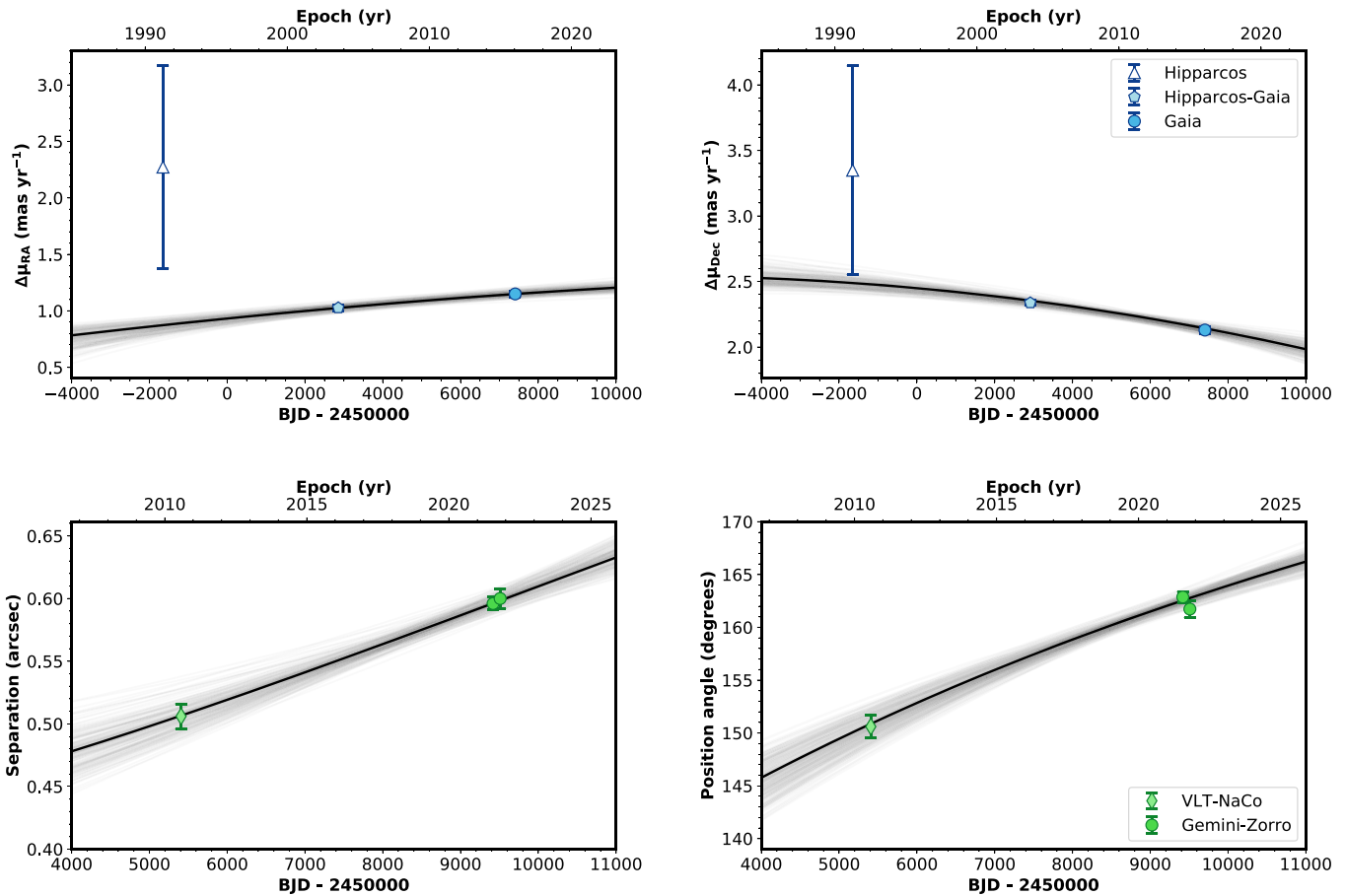


**Figure 14.** Gemini South Zorro speckle observations of HIP 94235 on 2021 October 22. The speckle auto cross correlation functions are shown in the top row, with the image from the blue camera at 562 nm on the left, and the red camera at 832 nm on the right. A companion is detected in the red arm with a contrast of  $\Delta m = 5.3$  at a separation of  $0''.6$ . No companions were detected on the blue arm with a limit of  $\Delta m > 4.7$ . The companion is marked in the red arm image.

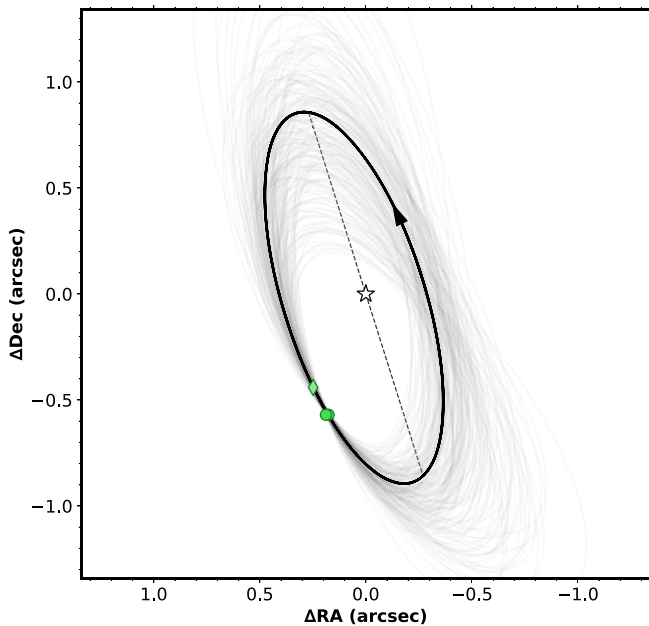
from the CHEOPS mission. We obtained five orbits of observations with CHEOPS to recover the transit of HIP 94235 b. Such follow-up would have been difficult to schedule with ground-based facilities due to the shallow transit.

Figure 6 demonstrates the importance of CHEOPS follow-up in preserving the transit timing ephemeris. Without such observations, the timing derived from the three transits observed in the single-sector TESS observation would have eroded by  $\sim 1$  hr per year. If a follow-up confirmation was not obtained within the first year after discovery, targeted transit observations would have been difficult to schedule and the recovery of such a small planet challenging (see Dragomir et al. 2020).

HIP 94235 b is one of the smallest planets that has been found transiting a young star. Figure 17 shows the position of



**Figure 15.** Keplerian orbital model to the proper motion of HIP 94235 (top left in R.A., top right in decl.) and relative astrometry of HIP 94235 B (bottom left in separation, bottom right in position angle). The best-fit model is shown in black, while the orbits in gray are drawn randomly from the posteriors. In the fit to the proper motions, all values are normalized to the proper motion of the system barycenter.



**Figure 16.** Projected sky orbit of HIP 94235 B. The data format is as in Figure 15. The dotted line marks the intersection of the planes of the orbit and of the sky and the black arrowhead indicates the direction of motion. Despite the short arc of observations our joint fit allows us to robustly constrain several orbital parameters, including strong constraints on the orbital inclination ( $i = 67^{+8}_{-2.9}$ ) and semimajor axis ( $a = 56^{+9}_{-7}$  au) of the binary.

HIP 94235 b in the distribution of small planets around young stars. Most TESS planets that transit young stars, including HIP 94235 b, have radii that place them above the radius valley delineated by Fulton et al. (2017) and Owen & Wu (2017). HIP 94235 b is at the edge of detectability for the TESS light curve of HIP 94235, and selection biases likely shape the current TESS distribution of young planets. However, Rizzuto et al. (2017) found young clusters and associations surveyed by *K2* hosted planets larger than the equivalent distribution about field stars. A similar holistic study of young stars surveyed by TESS may elucidate the radius evolution timescale for young planets.

Interestingly, despite continuous monitoring from the *K2* mission of  $\sim 1000$  Pleiades members, no confirmed planets have yet been found in the 125 Myr old cluster (e.g., Hartman et al. 2010; Rizzuto et al. 2017). Systems such as TOI-451 (Newton et al. 2021) in the Pisces–Eridanus stream (Meingast et al. 2019; Curtis et al. 2019), and HIP 94235 in AB Doradus, may help constrain the occurrence rates and radius properties of planets at the  $\sim 100$  Myr age range. These can help infer if the absence of planets in the Pleiades is due to detection biases, or if other astrophysical mechanisms may be at play.

Planets like HIP 94235 b, lying near the edge of the sub-Neptune valley, can provide key observational tests for the mechanisms of mass loss in young planets. HIP 94235 b and other recently discovered planets around young stars are subjected to significant high-energy radiation, which can be a dominant driver for rapid mass loss within the first hundreds of

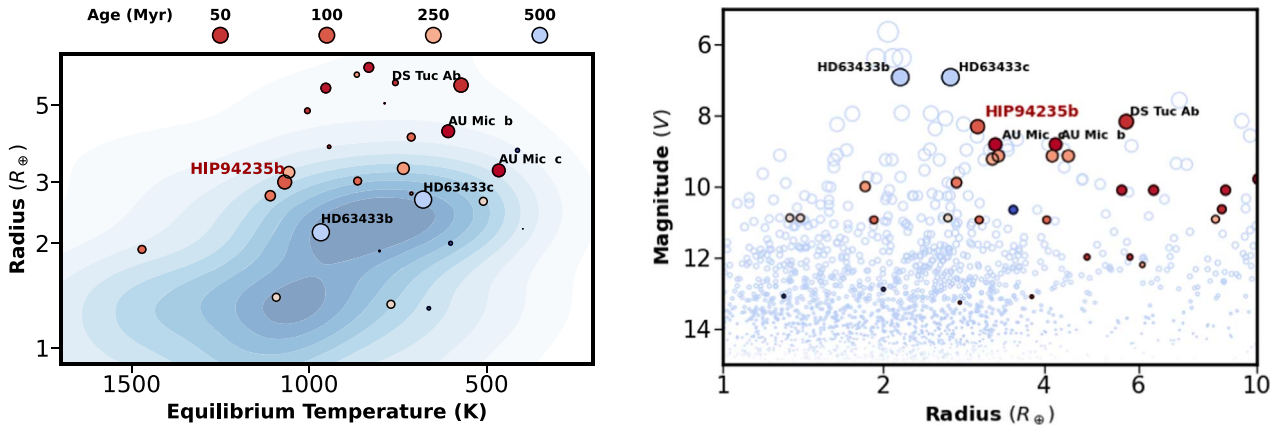


**Figure 17.** HIP 94235 b among the distribution of small planets. The left panel shows the radius and equilibrium temperature distribution of planets from Fulton et al. (2017). The sizes of each point mark the  $V$ -band magnitude of each host star, with the scale defined by the left panel. Planets around known young stars marked by the individual points. HIP 94235 b lies near the edge of the mini-Neptune desert. The right panel compares the planetary radius and host-star magnitude of HIP 94235 b compared to other systems. Young planets are highlighted. The cyan points mark other transiting systems from the NASA Exoplanet Archive (January 2021). Young systems included in the figure are TOI-1227 (Mann et al. 2022), V1298 Tau (David et al. 2019a, 2019b), K2-33 (Mann et al. 2016b; David et al. 2016), DS Tuc A (Benatti et al. 2019; Newton et al. 2019), Kepler-63 (Sanchis-Ojeda et al. 2013), HIP 67522 (Rizzuto et al. 2020), HD63433 (Mann et al. 2020), TOI-451 (Newton et al. 2021), AU Mic (Plavchan et al. 2020), TOI-251 (Zhou et al. 2021), TOI-942 (Carleo et al. 2021; Zhou et al. 2021), K2-284 (David et al. 2018a), TOI-837 (Bouma et al. 2020), TOI-1098 (Tofflemire et al. 2021), K2-233 (David et al. 2018b; Lillo-Box et al. 2020), K2-77 (Gaidos et al. 2017), K2-95, K2-100, K2-101, K2-102, K2-104, EPIC-211822797 (Mann et al. 2017), TOI-1807, TOI-2076 (Hedges et al. 2021), Kepler 1627A (Bouma et al. 2022), TOI-1268 (Dong et al. 2022).

millions of years post formation (Owen & Jackson 2012). To estimate the mass evolution of HIP 94235 b, we adopt the analytical approach from Owen & Wu (2017). We find that we can replicate the current radius of HIP 94235 b via a planet model that has a high initial envelope mass fraction, and undergoes rapid mass loss with a timescale of  $\sim 100\text{--}200$  Myr (Figure 18). HIP 94235 b has a current energy-limited mass-loss rate of  $\sim 5 M_{\oplus} \text{Gyr}^{-1}$ . At the end of this process, we expect the envelope mass fraction to reduce from 10% to  $\sim 1\%$  of the total planet mass. Such mass and radius evolution is expected for many close-in Neptunes and super-Earths around Sun-like stars.

Figure 19 shows the X-ray irradiation experienced by HIP 94235 b compared to other systems about X-ray sources identified in the Second ROSAT Point-source Catalog (Boller et al. 2016). To convert ROSAT count rates to fluxes, we adopt the calibration in Fleming et al. (1995) and parallaxes made available from Gaia Collaboration et al. (2018). The majority of planetary systems around ROSAT X-ray sources are young, and the recent TESS discoveries of nearby planet-hosting young stars are the most suitable targets for follow-up X-ray and UV observations. au Mic (Plavchan et al. 2020) has the highest ROSAT count rate for any planet-hosting star. Similarly, other nearby systems such as the planets around V1298 Tau (David et al. 2019a, 2019b), the ultrashort period super-Earth TOI-1807b (Hedges et al. 2021), DS Tuc Ab (Newton et al. 2019), and HIP 94235 b mark the inner boundary of X-ray irradiation for small planets. The only planets around stars not identified as young in literature residing in more energetic environments are the hot Jupiter NGTS-16b (Tilbrook et al. 2021) and the Earth-sized inner planet in the Kepler-1514 system (Dalba et al. 2021). Neither have radii susceptible to significant modification by photoevaporation. Recent observations by Zhang et al. (2022b) detected the Ly $\alpha$  transit of HD63433 c. Similar observations in the X-ray for young active stars have the potential of anchoring the photoevaporation models.

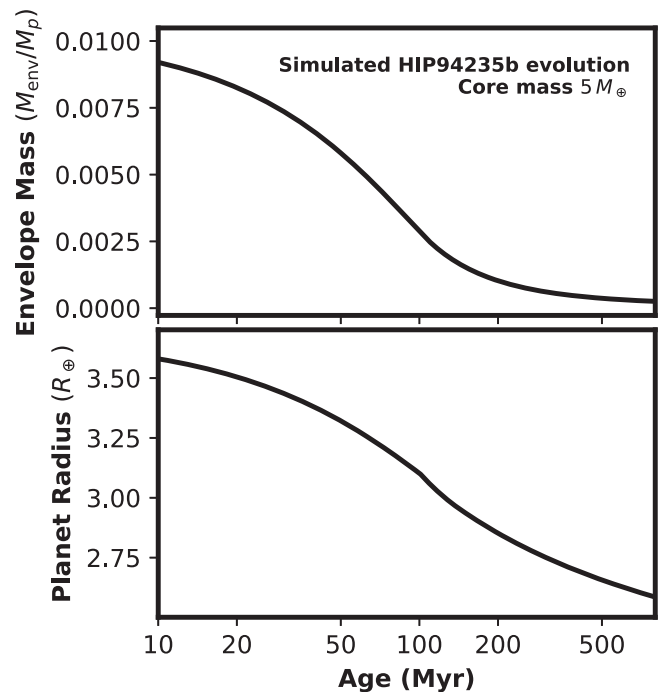


**Figure 18.** At 100 Myr, HIP 94235 is undergoing runaway mass-loss evolution. The top shows the mass evolution of primordial envelope for the planet as per Owen & Wu (2017). Within the first  $\sim 100$  Myr, HIP 94235 b is expected to lose most of its primordial envelope. The bottom panel shows the corresponding radius evolution expected for HIP 94235 b over the next few hundred million years.

Other avenues of mass loss are also possible. Atmospheric erosion from giant impact events can occur even more quickly, before compact super-Earth systems settle dynamically, acting on the tens of millions of years timescale post disk dispersal (e.g., Izidoro et al. 2017). Core-powered mass loss may also reproduce the observed radius distribution independent of the host-star irradiation (Lopez & Fortney 2013; Ginzburg et al. 2018). By



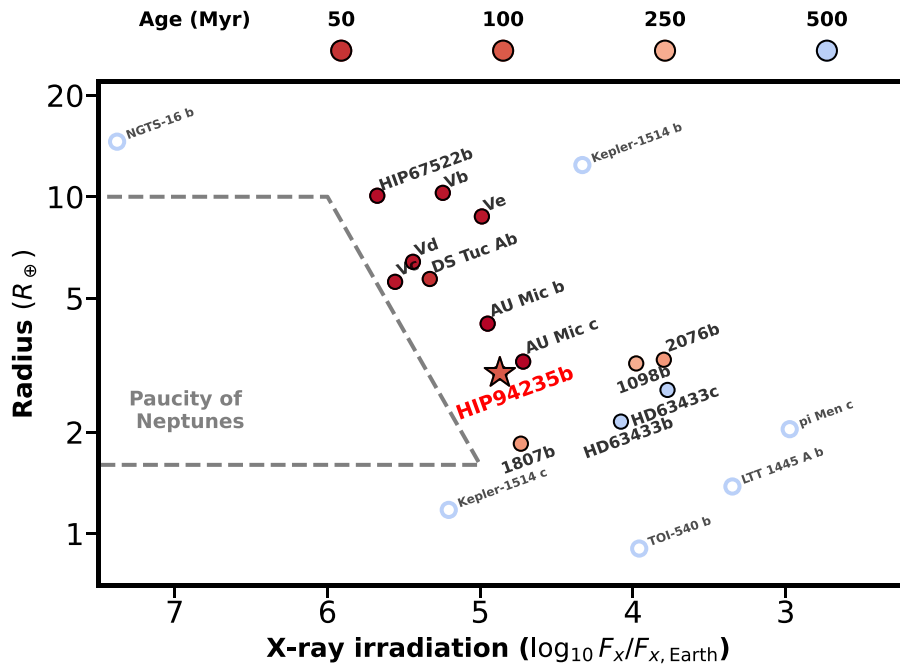


**Figure 19.** A large fraction of host stars that exhibit significant X-ray emission are known young stars. The X-ray irradiation received by all known transiting planets systems that have X-ray counterparts in the second ROSAT point-source catalog (Boller et al. 2016) are shown. We see a paucity of planets with radii between 2–10  $R_{\oplus}$  in energetic environments. Older systems are marked by open light blue points, planets around known young stars or association and cluster members are marked by closed points, with older systems in light blue, younger systems in red. For brevity, names with “TOI” have been truncated to their TOI numbers only, and the V1298 Tau system are denoted by “Vb”, “Vc”, “Vd”, “Ve”.

inferring the ages of Kepler systems through numerous indicators, David et al. (2021) found the radius gap may form at longer timescales. As such, it is unclear which mechanism dominates in shaping our current planet distribution.

At 50 au, HIP 94235 is one of the tightest stellar binaries (Su et al. 2021). Like the DS Tuc AB system (Newton et al. 2019), the orbit of the binary is aligned with that of the planetary orbit. This follows the trend from Christian et al. (2022) that wide transiting planet-hosting binaries with separations between 100–700 au are preferentially found in edge-on orbits. Christian et al. (2022) suggest that such trends may be due to the companions being formed from disk fragmentation, or the realignment of the inner disk by the perturbing outer companion. The efforts by TESS follow-up teams to provide diffraction limited imaging of a majority of planet candidates, such as HIP 94235, will help probe the continuation of this trend to <100 au separations.

The brightness of HIP 94235 makes the system suitable for follow-up atmospheric characterization with the next generation of space and ground-based facilities. Adopting the mass-radius relationship from Wolfgang et al. (2016), HIP 94235 b has a predicted mass of  $11.2 \pm 1.4 M_{\oplus}$ , yielding a transmission spectroscopic metric of  $96 \pm 25$ . As such, HIP 94235 b ranks among the top dozen known planets between 1.6–4  $R_{\oplus}$  in its suitability for follow-up transmission observations. In the era of JWST, we can compare the atmosphere of HIP 94235 b against planets of similar radii about older stars. We may find that young planets host primarily primordial atmospheres dominated by hydrogen and helium, with older planets hosting heavier water-rich atmospheres, or that some highly energetic environments may never allow secondary atmospheres to form. Orbital obliquities of young planets can help constrain the timescales of migration for planets that may have formed further out in their planetary systems. We expect a  $\sim 10 \text{ m s}^{-1}$

Rossiter–McLaughlin signal if HIP 94235 b is in a well-aligned projected orbit. The stellar activity will be a limiting factor in achieving a secure detection of the spectroscopic transit, though past works have shown that this can be mitigated on transit timescales due to the smoothly varying nature of the rotational modulated velocity noise (e.g., Palle et al. 2020; Benatti et al. 2021).



We respectfully acknowledge the traditional custodians of all lands throughout Australia, and recognize their continued cultural and spiritual connection to the land, waterways, cosmos, and community. We pay our deepest respects to all Elders, ancestors and descendants of the Giabal, Jarowair, and Kambuwal nations, upon whose lands the MINERVA-Australis facility at Mount Kent is situated. G.Z. thanks the support of the ARC DECRA program DE210101893. C.W. and G.Z. thank the support of the TESS Guest Investigator Program G03007. C.H. thanks the support of the ARC DECRA program DE200101840. E.G. gratefully acknowledges support from the David and Claudia Harding Foundation in the form of a Winton Exoplanet Fellowship. CHEOPS is an ESA mission in partnership with Switzerland with important contributions to the payload and the ground segment from Austria, Belgium, France, Germany, Hungary, Italy, Portugal, Spain, Sweden, and the United Kingdom. We thank support from the CHEOPS GO Programme and Science Operations Centre for help in the preparation and analysis of the CHEOPS observations. This research has used data from the CTIO/SMARTS 1.5 m telescope, which is operated as part of the SMARTS Consortium by RECONS. This study was based in part on observations made using the Las Cumbres Observatory global telescope network, using time allocated by the National Science Foundation’s NOIRLab (NOIRLab Prop. ID NOAO2021A-009; principal investigator: J. Hartman). Some of the






observations reported in this paper were obtained with the Southern African Large Telescope (SALT). Some of the observations in the paper made use of the high-resolution imaging instrument Zorro obtained under Gemini LLP Proposal Number: GN/S-2021A-LP-105. Zorro was funded by the NASA Exoplanet Exploration Program and built at the NASA Ames Research Center by Steve B. Howell, Nic Scott, Elliott P. Horch, and Emmett Quigley. Zorro was mounted on the Gemini North (and/or South) telescope of the international Gemini Observatory, a program of NSF's OIR Lab, which is managed by the Association of Universities for Research in Astronomy (AURA) under a cooperative agreement with the National Science Foundation on behalf of the Gemini partnership: the National Science Foundation (United States), National Research Council (Canada), Agencia Nacional de Investigación y Desarrollo (Chile), Ministerio de Ciencia, Tecnología e Innovación (Argentina), Ministério da Ciência, Tecnologia, Inovações e Comunicações (Brazil), and Korea Astronomy and Space Science Institute (Republic of Korea). This research has made use of the NASA Exoplanet Archive, which is operated by the California Institute of Technology, under contract with the National Aeronautics and Space Administration under the Exoplanet Exploration Program. Funding for the TESS mission is provided by NASA's Science Mission directorate. We acknowledge the use of public TESS Alert data from pipelines at the TESS Science Office and at the TESS Science Processing Operations Center. This research has made use of the Exoplanet Follow-up Observation Program website, which is operated by the California Institute of Technology, under contract with the National Aeronautics and Space Administration under the Exoplanet Exploration Program. This paper includes data collected by the TESS mission, which are publicly available from the Mikulski Archive for Space Telescopes (MAST). Resources supporting this work were provided by the NASA High-End Computing (HEC) program through the NASA Advanced Supercomputing (NAS) Division at Ames Research Center for the production of the SPOC data products. MINERVA-Australis is supported by Australian Research Council LIEF Grant LE160100001, Discovery Grants DP180100972 and DP220100365, Mount Cuba Astronomical Foundation, and institutional partners University of Southern Queensland, UNSW Sydney, MIT, Nanjing University, George Mason University, University of Louisville, University of California Riverside, University of Florida, and The University of Texas at Austin. D.D. acknowledges support from the TESS Guest Investigator Program grants 80NSSC21K0108 and 80NSSC22K0185.

*Facility:* TESS, CHEOPS, Exoplanet Archive, CTIO 1.5 m, LCOGT, Gemini:Zorro, SALT, MINERVA-Australis.

*Software:* emcee (Foreman-Mackey et al. 2013), batman (Kreidberg 2015), astropy (Astropy Collaboration et al. 2018), PyAstronomy (Czesla et al. 2019), comove (Tofflemire et al. 2021).

### ORCID iDs

George Zhou  <https://orcid.org/0000-0002-4891-3517>  
 Christopher P. Wirth  <https://orcid.org/0000-0003-1656-011X>  
 Chelsea X. Huang  <https://orcid.org/0000-0003-0918-7484>  
 Alexander Venner  <https://orcid.org/0000-0002-8400-1646>  
 Samuel N. Quinn  <https://orcid.org/0000-0002-8964-8377>  
 L. G. Bouma  <https://orcid.org/0000-0002-0514-5538>

Adam L. Kraus  <https://orcid.org/0000-0001-9811-568X>  
 Andrew W. Mann  <https://orcid.org/0000-0003-3654-1602>  
 Elisabeth. R. Newton  <https://orcid.org/0000-0003-4150-841X>  
 Diana Dragomir  <https://orcid.org/0000-0003-2313-467X>  
 Alexis Heitzmann  <https://orcid.org/0000-0002-8091-7526>  
 Natalia Lowson  <https://orcid.org/0000-0001-6508-5736>  
 Stephanie T. Douglas  <https://orcid.org/0000-0001-7371-2832>  
 Matthew Battley  <https://orcid.org/0000-0002-1357-9774>  
 Edward Gillen  <https://orcid.org/0000-0003-2851-3070>  
 Amaury Triaud  <https://orcid.org/0000-0002-5510-8751>  
 David W. Latham  <https://orcid.org/0000-0001-9911-7388>  
 Steve B. Howell  <https://orcid.org/0000-0002-2532-2853>  
 J. D. Hartman  <https://orcid.org/0000-0001-8732-6166>  
 Benjamin M. Tofflemire  <https://orcid.org/0000-0003-2053-0749>  
 Robert A. Wittenmyer  <https://orcid.org/0000-0001-9957-9304>  
 Brendan P. Bowler  <https://orcid.org/0000-0003-2649-2288>  
 Jonathan Horner  <https://orcid.org/0000-0002-1160-7970>  
 Stephen R. Kane  <https://orcid.org/0000-0002-7084-0529>  
 John Kielkopf  <https://orcid.org/0000-0003-0497-2651>  
 Peter Plavchan  <https://orcid.org/0000-0002-8864-1667>  
 Duncan J. Wright  <https://orcid.org/0000-0001-7294-5386>  
 Brett C. Addison  <https://orcid.org/0000-0003-3216-0626>  
 Matthew W. Mengel  <https://orcid.org/0000-0002-7830-6822>  
 George Ricker  <https://orcid.org/0000-0003-2058-6662>  
 Roland Vanderspek  <https://orcid.org/0000-0001-6763-6562>  
 Sara Seager  <https://orcid.org/0000-0002-6892-6948>  
 Jon M. Jenkins  <https://orcid.org/0000-0002-4715-9460>  
 Joshua N. Winn  <https://orcid.org/0000-0002-4265-047X>  
 Tansu Daylan  <https://orcid.org/0000-0002-6939-9211>  
 Michael Fausnaugh  <https://orcid.org/0000-0002-9113-7162>  
 Michelle Kunimoto  <https://orcid.org/0000-0001-9269-8060>

### References

- Addison, B., Wright, D. J., Wittenmyer, R. A., et al. 2019, *PASP*, 131, 115003  
 Allart, R., Bourrier, V., Lovis, C., et al. 2019, *A&A*, 623, A58  
 Astropy Collaboration, Price-Whelan, A. M., Sipőcz, B. M., et al. 2018, *AJ*, 156, 123  
 Barenfeld, S. A., Bubar, E. J., Mamajek, E. E., & Young, P. A. 2013, *ApJ*, 766, 6  
 Barrado y Navascués, D., Stauffer, J. R., & Jayawardhana, R. 2004, *ApJ*, 614, 386  
 Barragán, O., Aigrain, S., Kubyskhina, D., et al. 2019, *MNRAS*, 490, 698  
 Bell, C. P. M., Mamajek, E. E., & Naylor, T. 2015, *MNRAS*, 454, 593  
 Benatti, S., Nardiello, D., Malavolta, L., et al. 2019, *A&A*, 630, A81  
 Benatti, S., Damasso, M., Borsa, F., et al. 2021, *A&A*, 650, A66  
 Benz, W., Broeg, C., Fortier, A., et al. 2021, *ExA*, 51, 109  
 Blunt, S., Nielsen, E. L., De Rosa, R. J., et al. 2017, *AJ*, 153, 229  
 Blunt, S., Wang, J. J., Angelo, I., et al. 2020, *AJ*, 159, 89  
 Boller, T., Freyberg, M. J., Trümper, J., et al. 2016, *A&A*, 588, A103  
 Bouma, L. G., Hartman, J. D., Brahm, R., et al. 2020, *AJ*, 160, 239  
 Bouma, L. G., Curtis, J. L., Masuda, K., et al. 2022, *AJ*, 163, 121  
 Bourrier, V., Lecavelier des Etangs, A., Ehrenreich, D., et al. 2018, *A&A*, 620, A147  
 Bowler, B. P., Cochran, W. D., Endl, M., et al. 2021, *AJ*, 161, 106  
 Brandt, T. D. 2018, *ApJS*, 239, 31  
 Brandt, T. D. 2021, *ApJS*, 254, 42  
 Brandt, T. D., Dupuy, T. J., & Bowler, B. P. 2019, *AJ*, 158, 140  
 Brandt, T. D., & Huang, C. X. 2015, *ApJ*, 807, 58  
 Brown, T. M., Baliber, N., Bianco, F. B., et al. 2013, *PASP*, 125, 1031  
 Buchhave, L. A., Latham, D. W., Johansen, A., et al. 2012, *Natur*, 486, 375  
 Buckley, D. A. H., Swart, G. P., & Meiring, J. G. 2006, *Proc. SPIE*, 6267, 62670Z

- Burke, C. J., Christiansen, J. L., Mullally, F., et al. 2015, *ApJ*, 809, 8
- Calissendorff, P., & Janson, M. 2018, *A&A*, 615, A149
- Carleo, I., Desidera, S., Nardiello, D., et al. 2021, *A&A*, 645, A71
- Castelli, F., & Kurucz, R. L. 2004, arXiv:astro-ph/0405087
- Chauvin, G., Vigan, A., Bonnefoy, M., et al. 2015, *A&A*, 573, A127
- Choi, J., Dotter, A., Conroy, C., et al. 2016, *ApJ*, 823, 102
- Christian, S., Vanderburg, A., Becker, J., et al. 2022, *AJ*, 163, 207
- Claret, A. 2017, *A&A*, 600, A30
- Claret, A., & Bloemen, S. 2011, *A&A*, 529, A75
- Crause, L. A., Sharples, R. M., Bramall, D. G., et al. 2014, *Proc. SPIE*, 9147, 91476T
- Curtis, J. L., Agüeros, M. A., Mamajek, E. E., Wright, J. T., & Cummings, J. D. 2019, *AJ*, 158, 77
- Cutri, R. M., Wright, E. L., Conrow, T., et al. 2012, *yCat*, 2320, 0
- Czesla, S., Schröter, S., Schneider, C. P., et al. 2019, PyA: Python astronomy-related packages, Astrophysics Source Code Library, ascl:1906.010
- da Silva, L., Torres, C. A. O., de La Reza, R., et al. 2009, *A&A*, 508, 833
- Dalba, P. A., Kane, S. R., Isaacson, H., et al. 2021, *AJ*, 161, 103
- David, T. J., Petigura, E. A., Luger, R., et al. 2019a, *ApJL*, 885, L12
- David, T. J., Hillenbrand, L. A., Petigura, E. A., et al. 2016, *Natur*, 534, 658
- David, T. J., Mamajek, E. E., Vanderburg, A., et al. 2018a, *AJ*, 156, 302
- David, T. J., Crossfield, I. J. M., Benneke, B., et al. 2018b, *AJ*, 155, 222
- David, T. J., Cody, A. M., Hedges, C. L., et al. 2019b, *AJ*, 158, 79
- David, T. J., Contardo, G., Sandoval, A., et al. 2021, *AJ*, 161, 265
- Desidera, S., Covino, E., Messina, S., et al. 2015, *A&A*, 573, A126
- Dong, J., Huang, C. X., Zhou, G., et al. 2022, *ApJL*, 926, L7
- Dotter, A. 2016, *ApJS*, 222, 8
- Dragomir, D., Harris, M., Pepper, J., et al. 2020, *AJ*, 159, 219
- Ehrenreich, D., Bourrier, V., Bonfils, X., et al. 2012, *A&A*, 547, A18
- Ehrenreich, D., Bourrier, V., Wheatley, P. J., et al. 2015, *Natur*, 522, 459
- ESA 1997, ESA SP-1200, The HIPPARCOS and TYCHO Catalogues (Noordwijk: ESA)
- Feinstein, A. D., Montet, B. T., Johnson, M. C., et al. 2021, *AJ*, 162, 213
- Fleming, T. A., Schmitt, J. H. M. M., & Giampapa, M. S. 1995, *ApJ*, 450, 401
- Foreman-Mackey, D., Agol, E., Angus, R., & Ambikasaran, S. 2017, *AJ*, 154, 220
- Foreman-Mackey, D., Hogg, D. W., Lang, D., & Goodman, J. 2013, *PASP*, 125, 306
- Fulton, B. J., Petigura, E. A., Howard, A. W., et al. 2017, *AJ*, 154, 109
- Gagné, J., Faherty, J. K., Moranta, L., & Popinchalk, M. 2021, *ApJL*, 915, L29
- Gagné, J., Mamajek, E. E., Malo, L., et al. 2018, *ApJ*, 856, 23
- Gaia Collaboration, Brown, A. G. A., Vallenari, A., et al. 2018, *A&A*, 616, A1
- Gaia Collaboration, Brown, A. G. A., Vallenari, A., et al. 2021, *A&A*, 649, A1
- Gaidos, E., Mann, A. W., Rizzuto, A., et al. 2017, *MNRAS*, 464, 850
- Gaidos, E., Hirano, T., Beichman, C., et al. 2022, *MNRAS*, 509, 2969
- Ginzburg, S., Schlichting, H. E., & Sari, R. 2018, *MNRAS*, 476, 759
- Gupta, A., & Schlichting, H. E. 2021, *MNRAS*, 504, 4634
- Hartman, J. D., Bakos, G. Á., Kovács, G., & Noyes, R. W. 2010, *MNRAS*, 408, 475
- Hedges, C., Hughes, A., Zhou, G., et al. 2021, *AJ*, 162, 54
- Henden, A. A., Templeton, M., Terrell, D., et al. 2016, *yCat*, II, 336
- Howell, S. B., Everett, M. E., Horch, E. P., et al. 2016, *ApJL*, 829, L2
- Howell, S. B., Everett, M. E., Sherry, W., Horch, E., & Ciardi, D. R. 2011, *AJ*, 142, 19
- Howell, S. B., Sobeck, C., Haas, M., et al. 2014, *PASP*, 126, 398
- Hoyer, S., Guterman, P., Demangeon, O., et al. 2020, *A&A*, 635, A24
- Huang, C. X., Vanderburg, A., Pál, A., et al. 2020a, *RNAAS*, 4, 204
- Huang, C. X., Vanderburg, A., Pál, A., et al. 2020b, *RNAAS*, 4, 206
- Inamdar, N. K., & Schlichting, H. E. 2015, *MNRAS*, 448, 1751
- Izidoro, A., Ogihara, M., Raymond, S. N., et al. 2017, *MNRAS*, 470, 1750
- Jenkins, J. M., Twicken, J. D., McCauliff, S., et al. 2016, *Proc. SPIE*, 9913, 99133E
- Kervella, P., Arenou, F., Mignard, F., & Thévenin, F. 2019, *A&A*, 623, A72
- Kirk, J., Alam, M. K., López-Morales, M., & Zeng, L. 2020, *AJ*, 159, 115
- Kite, E. S., & Barnett, M. N. 2020, *PNAS*, 117, 18264
- Kniazhev, A. Y., Gvaramadze, V. V., & Berdnikov, L. N. 2016, *MNRAS*, 459, 3068
- Kniazhev, A. Y., Gvaramadze, V. V., & Berdnikov, L. N. 2017, in *Stars: From Collapse to Collapse* (San Francisco, CA: ASP), 480
- Kounkel, M., & Covey, K. 2019, *AJ*, 158, 122
- Kovács, G., Zucker, S., & Mazeh, T. 2002, *A&A*, 391, 369
- Kreidberg, L. 2015, *PASP*, 127, 1161
- Kulow, J. R., France, K., Linsky, J., & Loyd, R. O. P. 2014, *ApJ*, 786, 132
- Lavie, B., Ehrenreich, D., Bourrier, V., et al. 2017, *A&A*, 605, L7
- Lee, E. J., & Connors, N. J. 2021, *ApJ*, 908, 32
- Lee, E. J., Karalis, A., & Thorngren, D. P. 2022, arXiv:2201.09898
- Lightkurve Collaboration, Cardoso, J. V. D. M., Hedges, C., et al. 2018, Lightkurve: Kepler and TESS time series analysis in Python, Astrophysics Source Code Library, ascl:1812.013
- Lillo-Box, J., Lopez, T. A., Santerne, A., et al. 2020, *A&A*, 640, 48
- Livingston, J. H., Dai, F., Hirano, T., et al. 2019, *MNRAS*, 484, 8
- Lopez, E. D., & Fortney, J. J. 2013, *ApJ*, 776, 2
- Lopez, E. D., Fortney, J. J., & Miller, N. 2012, *ApJ*, 761, 59
- Luhman, K. L., Stauffer, J. R., & Mamajek, E. E. 2005, *ApJL*, 628, L69
- Malo, L., Doyon, R., Lafrenière, D., et al. 2013, *ApJ*, 762, 88
- Mamajek, E. E., & Hillenbrand, L. A. 2008, *ApJ*, 687, 1264
- Mandel, K., & Agol, E. 2002, *ApJL*, 580, L171
- Mann, A. W., Gaidos, E., Mace, G. N., et al. 2016a, *ApJ*, 818, 46
- Mann, A. W., Newton, E. R., Rizzuto, A. C., et al. 2016b, *AJ*, 152, 61
- Mann, A. W., Gaidos, E., Vanderburg, A., et al. 2017, *AJ*, 153, 64
- Mann, A. W., Johnson, M. C., Vanderburg, A., et al. 2020, *AJ*, 160, 179
- Mann, A. W., Wood, M. L., Schmidt, S. P., et al. 2022, *AJ*, 163, 156
- Marcus, R. A., Stewart, S. T., Sasselov, D., & Hernquist, L. 2009, *ApJL*, 700, L118
- Masuda, K., & Winn, J. N. 2020, *AJ*, 159, 81
- Maxted, P. F. L., Ehrenreich, D., Wilson, T. G., et al. 2021, arXiv:2111.08828
- Meingast, S., Alves, J., & Fűrnkranz, V. 2019, *A&A*, 622, L13
- Meynet, G., Mermilliod, J. C., & Maeder, A. 1993, *A&AS*, 98, 477
- Morris, R. L., Twicken, J. D., Smith, J. C., et al. 2020, Kepler Data Processing Handbook: Photometric Analysis, Kepler Data Processing Handbook (KSCI-19081-003)
- Newton, E. R., Mann, A. W., Tofflemire, B. M., et al. 2019, *ApJL*, 880, L17
- Newton, E. R., Mann, A. W., Kraus, A. L., et al. 2021, *AJ*, 161, 65
- Ortega, V. G., Jilinski, E., de La Reza, R., & Bazzanella, B. 2007, *MNRAS*, 377, 441
- Owen, J. E., & Jackson, A. P. 2012, *MNRAS*, 425, 2931
- Owen, J. E., & Wu, Y. 2013, *ApJ*, 775, 105
- Owen, J. E., & Wu, Y. 2017, *ApJ*, 847, 29
- Palle, E., Oshagh, M., Casasayas-Barris, N., et al. 2020, *A&A*, 643, A25
- Paredes, L. A., Henry, T. J., Quinn, S. N., et al. 2021, *AJ*, 162, 176
- Perryman, M. A. C., Lindegren, L., Kovalevsky, J., et al. 1997, *A&A*, 500, 501
- Petigura, E. A., Howard, A. W., & Marcy, G. W. 2013, *PNAS*, 110, 19273
- Plavchan, P., Barclay, T., Gagné, J., et al. 2020, *Natur*, 582, 497
- Pourbaix, D. 1998, *A&AS*, 131, 377
- Quinn, S. N., White, R. J., Latham, D. W., et al. 2012, *ApJL*, 756, L33
- Quinn, S. N., White, R. J., Latham, D. W., et al. 2014, *ApJ*, 787, 27
- Rebull, L. M., Stauffer, J. R., Hillenbrand, L. A., et al. 2017, *ApJ*, 839, 92
- Rebull, L. M., Stauffer, J. R., Bouvier, J., et al. 2016, *AJ*, 152, 113
- Ricker, G. R., Winn, J. N., Vanderspek, R., et al. 2015, *JATIS*, 1, 014003
- Rizzuto, A. C., Mann, A. W., Vanderburg, A., Kraus, A. L., & Covey, K. R. 2017, *AJ*, 154, 224
- Rizzuto, A. C., Vanderburg, A., Mann, A. W., et al. 2018, *AJ*, 156, 195
- Rizzuto, A. C., Newton, E. R., Mann, A. W., et al. 2020, *AJ*, 160, 33
- Rockcliffe, K. E., Newton, E. R., Youngblood, A., et al. 2021, *AJ*, 162, 116
- Sanchis-Ojeda, R., Winn, J. N., Marcy, G. W., et al. 2013, *ApJ*, 775, 54
- Skrutskie, M. F., Cutri, R. M., Stiening, R., et al. 2006, *AJ*, 131, 1163
- Snellen, I. A. G., & Brown, A. G. A. 2018, *NatAs*, 2, 883
- Soderblom, D. R. 2010, *ARA&A*, 48, 581
- Spake, J. J., Sing, D. K., Evans, T. M., et al. 2018, *Natur*, 557, 68
- Stassun, K. G., Oelkers, R. J., Pepper, J., et al. 2018, *AJ*, 156, 102
- Stauffer, J. R., Schultz, G., & Kirkpatrick, J. D. 1998, *ApJL*, 499, L199
- Su, X.-N., Xie, J.-W., Zhou, J.-L., & Thebault, P. 2021, *AJ*, 162, 272
- Tilbrook, R. H., Burleigh, M. R., Costes, J. C., et al. 2021, *MNRAS*, 504, 6018
- Tofflemire, B. M., Rizzuto, A. C., Newton, E. R., et al. 2021, *AJ*, 161, 171
- Tokovinin, A., Fischer, D. A., Bonati, M., et al. 2013, *PASP*, 125, 1336
- Twicken, J. D., Clarke, B. D., Bryson, S. T., et al. 2010, *Proc. SPIE*, 7740, 774023
- Ujjwal, K., Kartha, S. S., Mathew, B., Manoj, P., & Narang, M. 2020, *AJ*, 159, 166
- Vanderburg, A. 2021, avanderburg/edmcmc: v1.0.0, Zenodo, doi:10.5281/zenodo.5599854
- Vanderburg, A., & Johnson, J. A. 2014, *PASP*, 126, 948
- Vanderburg, A., Mann, A. W., Rizzuto, A., et al. 2018, *AJ*, 156, 46
- Vanderburg, A., Huang, C. X., Rodriguez, J. E., et al. 2019, *ApJL*, 881, L19
- Venner, A., Pearce, L. A., & Vanderburg, A. 2021a, arXiv:2111.03676
- Venner, A., Vanderburg, A., & Pearce, L. A. 2021b, *AJ*, 162, 12
- Wolfgang, A., Rogers, L. A., & Ford, E. B. 2016, *ApJ*, 825, 19
- Zhang, M., Knutson, H. A., Wang, L., Dai, F., & Barragán, O. 2022a, *AJ*, 163, 67
- Zhang, M., Knutson, H. A., Wang, L., et al. 2022b, *AJ*, 163, 68
- Zhou, G., Quinn, S. N., Irwin, J., et al. 2021, *AJ*, 161, 2
- Zhu, W., Petrovich, C., Wu, Y., Dong, S., & Xie, J. 2018, *ApJ*, 860, 101
- Zuckerman, B., Song, I., & Bessell, M. S. 2004, *ApJL*, 613, L65